inorganics

MDPI

Review

Progress in 2D MoS_2-Based Advanced Materials for Hydrogen Evolution and Energy Storage Applications

Waseem Raza [1,*,†], Khursheed Ahmad [2,†], Flaviano Garcia Alvarado [1] and Tae Hwan Oh [2,*]

[1] Department of Chemistry and Biochemistry, Facultad de Farmacia, Universidad San Pablo-CEU, CEU Universities, Urbanización Montepríncipe, Boadilla del Monte, 28668 Madrid, Spain; flaga@ceu.es
[2] School of Chemical Engineering, Yeungnam University, Gyeongsan 38541, Republic of Korea; khursheed@yu.ac.kr
* Correspondence: waseem.raza@ceu.es (W.R.); taehwanhoh@ynu.ac.kr (T.H.O.)
† These authors contributed equally to this work.

Abstract: The increasing energy demand for and fast depletion of fossil fuels have driven the need to explore renewable and clean energy sources. Hydrogen production via water electrocatalysis is considered a promising green fuel technology for addressing global energy and environmental challenges while supporting sustainable development. Molybdenum disulfide (MoS_2) has emerged as a potential electrocatalyst for hydrogen evolution reactions (HERs) and super-capacitor (SC) applications due to its high electrochemical activity, low cost, and abundance. However, compared to noble metals like platinum (Pt), MoS_2 exhibit lower HER activity in water electrocatalysis. Therefore, further modification is needed to enhance its catalytic performance. To address this, MoS_2 has been effectively modified with materials such as reduced graphene oxide (rGO), carbon nanotubes (CNTs), polymers, metal oxides, and MXenes. These modifications significantly improve the electrochemical properties of MoS_2, enhancing its performance in HER and SC applications. In this review article, we have compiled recent reports on the fabrication of MoS_2-based hybrid materials for HER and SC applications. The challenges, advantages, and future perspectives of MoS_2-based materials for HERs and SCs have been discussed. It is believed that readers may benefit from the recent updates on the fabrication of MoS_2-based hybrid materials for HER and SC applications.

Keywords: 2D materials; MoS_2; hydrogen evolution; energy storage

check for updates

Academic Editors: Torben R. Jensen, Hai-Wen Li, Terry Humphries, Mark Paskevicius and Craig Buckley

Received: 30 December 2024
Revised: 30 January 2025
Accepted: 2 February 2025
Published: 6 February 2025

Citation: Raza, W.; Ahmad, K.; Alvarado, F.G.; Oh, T.H. Progress in 2D MoS_2-Based Advanced Materials for Hydrogen Evolution and Energy Storage Applications. *Inorganics* **2025**, *13*, 47. https://doi.org/10.3390/inorganics13020047

Copyright: © 2025 by the authors. Licensee MDPI, Basel, Switzerland. This article is an open access article distributed under the terms and conditions of the Creative Commons Attribution (CC BY) license (https://creativecommons.org/licenses/by/4.0/).

1. Introduction

Humanity is currently facing two major challenges: energy and environmental crises. These issues arise from rapid population growth, advances in living standards, and uncontrolled industrial development leading to a global energy crisis [1–5]. The increasing global energy demand is mainly fulfilled by the use of fossil fuels. However, their excessive use has led to significant negative impacts on human health and the environment, particularly in developing countries [6,7]. Furthermore, the extensive use and burning of fossil fuels release significant amounts of different harmful gasses such as CO, CO_2, Sox, and NOx into the atmosphere, contributing to environmental pollution [1]. Therefore, it is crucial to develop eco-friendly and sustainable alternatives to meet the energy demand of the fast-growing population and rising living standards, while addressing environmental pollution and ensuring the sustainable development of global economy [2,8]. At this critical juncture, among all renewable energy sources, sustainable hydrogen energy is considered as the most promising ideal and alternative energy carrier to fossil fuels due to its high

energy capacity and environmentally friendly nature [9]. Moreover, hydrogen energy is also considered a green fuel because its combustion produces only water as a byproduct, which is non-polluting and does not contribute any environmental problems [10]. However, hydrogen is currently produced at the industrial level mainly through methane reforming or coal gasification. These processes release large amounts of greenhouse gases into the atmosphere, posing a significant amount of environmental challenges [9,10]. For the production of hydrogen via electrochemical water splitting, using electricity from renewable sources such as solar, wind, and tidal energy is one of the best methods that results in high-purity hydrogen [11]. This process is environmentally friendly, feasible, and cost-effective, providing a sustainable method for producing hydrogen fuel to meet global energy demands while addressing environmental problems [11]. Generally, the electrocatalysis and water splitting processes involve the decomposition of hydrogen and oxygen bonds in water, converting hydrogen bonds into hydrogen fuel [12]. This process consists of two key electrochemical half-reactions, such as hydrogen evolution reactions (HERs) at the cathode and oxygen evolution reactions (OERs) at the anode [13]. However, the splitting of water is an energy-intensive reaction with slow kinetics, which needs a large overpotential and high energy consumption, limiting its industrial application [14,15]. To make this process feasible for practical application, highly efficient electrocatalysts are essential for both HERs and OERs to enhance the activity and overall performance [15]. The theoretical overpotential for electrochemical water splitting is 1.23 V, but to effectively split water, an overpotential of around 1.8–2.0 V is needed, which is 1.5–1.6 times higher than the theoretical value [16]. Therefore, designing the effective electrocatalysts to reduce the overpotential of water splitting is crucial for enabling the efficient utilization of energy. At present, the most effective catalyst for electrocatalytic HERs is precious noble metal platinum (Pt), which can almost reach the theoretical decomposition overpotential of water splitting [17]. But the high cost and scarcity of Pt limits its industrial application [17]. Therefore, developing high-performance HER electrocatalysts with low costs and abundant reserves is crucial but challenging. To achieve this, significant efforts have been dedicated to reducing the overpotential of slow HER kinetics by employing non-Pt transitions metal electrocatalysts, including carbides, sulfides, borides, nitrides, and phosphides [18–22].

In recent days, transition metal dichalcogenides (TMDs), such as WS_2, WSe_2, MoS_2, $MoSe_2$, etc., have been extensively utilized in sensors, electronics, and the catalysis field owing to its outstanding electronic and chemical properties [23–25]. Among TMDs, MoS_2 has gained significant attention in the field of electrocatalysis due to its low cost, low toxicity, high durability, and unique physicochemical properties [24,25].

As a typical two-dimensional (2D) material, MoS_2, has been widely studied as a potential HER catalyst, demonstrating great potential to replace Pt both theoretically and experimentally [9]. This is primarily due to its nearly ideal theoretical hydrogen adsorption Gibbs free energy (ΔG_H = 0.06 eV), which is close to zero, making it highly effective for HERs [26]. In a typical lamellar hexagonal structure, the atomic layers of MoS_2 are arranged in such a way that each monolayer is covalently bonded via Mo-S-Mo bonds, whereas adjacent layers interact through van der Walls forces [9,27]. In general, within each MoS_2, the Mo atoms are covalently bonded to six adjacent sulfur atoms, and there are no dangling bonds between layers, other than van del Walls interactions. The different stacking arrangements of Mo and S layers give rise to different crystal phases, such as 1T, 2H, and 3R. For catalysis applications, the 1T and 2H phases of MoS_2 have been extensively studied and compared [28,29]. MoS_2 naturally occurs in the 2H phase, showing a 2D lamellar structure similar to graphite, with layers connected by van der Walls forces [9,30]. The 2H phase is characterized by a triangular prismatic structure, exhibiting semiconducting properties, and is thermodynamically stable. Each monolayer consists of three atomic

layers in an S-Mo-S arrangement, where two S layers are symmetrically positioned and the Mo atom resides at the center of the triangular prism formed by the S atoms. The Mo atom is coordinated with the surrounding six S atoms [9,31]. In the 2H phase of MoS_2, the symbol "2" signifies the structural periodicity, indicating that two layers of S-Mo-S monolayers are repetitively stacked as a structural unit, whereas the symbol "H" denotes the hexagonal crystal system, reflecting the coordination structure of the material. The 1T phase of MoS_2 also possesses a 2D structure but differs in its octahedral coordination. This phase is thermodynamically metastable and exhibits metallic properties, making it distinct from the semiconducting 2H phase [32]. Each monolayer is composed of three atomic layers of S-Mo-S atoms, where two S layers are asymmetrically positioned and the Mo atom is sandwiched between two layers of S atoms. The 1T phase of the MoS_2 structure can be obtained by rotating the S atomic layer by 60° around the center of the top plane, using the triangular prism structure of the 2H phase as a reference [33]. In this configuration, each Mo atom is octahedrally coordinated with six S atoms, which is denoted by the "T" in 1T, referring to trigonal. The 1T phase of MoS_2 is constructed by the repeated stacking of single atomic layers along the *c*-axis, with each layer serving as a fundamental unit, as indicated by the "1" in 1T [34]. Figure 1 illustrates the 2H and 1T phases of MoS_2. The distinct crystalline phases of MoS_2 exhibit varying properties due to the differences in their structural configurations. However, in the case of the 3R phase, the arrangement of the scaring method is the same as for 2H phase of S-Mo-S, but the Mo atoms occupy the center of triangular prisms [33]. The main structural distinction between the 2H and 3R phases lies in the layer arrangement along the *c*-axis. The 2H phase contains two layers per unit cell, whereas the 3R phase contains three layers per unit cell. Moreover, the 3R-type phase of MoS_2 readily transforms into a more thermodynamically stable 2H phase upon heating [34].

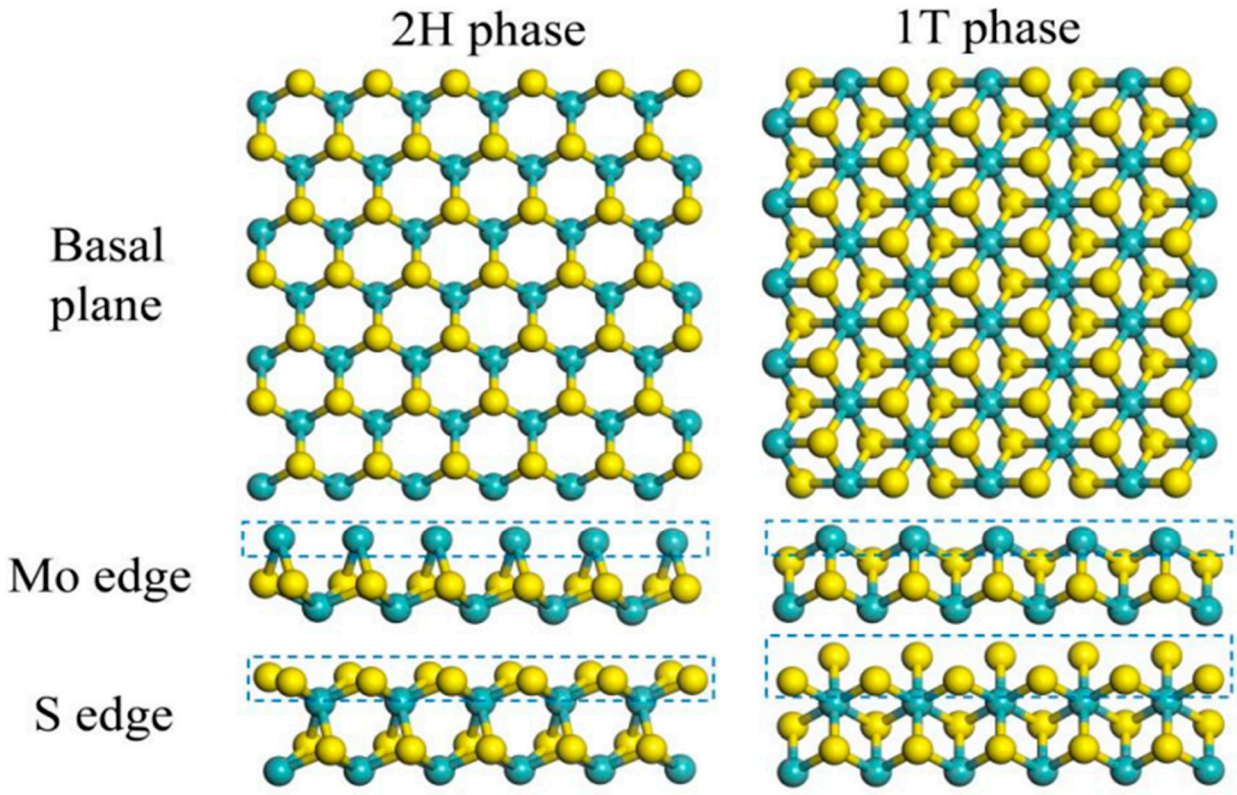

Figure 1. The typical ball and stick model of the 2H and 1T phases of MoS_2, where pale blue represents Mo atoms and the yellow color denotes S atoms. Reproduced with permission from Ref. [35], copyright 2024, MDPI.

Over the past decades, numerous studies have been conducted to achieve high HER activity using MoS_2. However, its performance remains significantly lower than the Pt catalyst due to MoS_2's low conductivity and inert basal planes. Early research by Tributsch and Bennett on bulk MoS_2 demonstrated that this is not an efficient HER catalyst [36]. Subsequently, in 2005, groundbreaking work by Hinnemann and co-workers revealed that the nanostructure of MoS_2 exhibits significantly improved HER activity [37]. This improvement is attributed to the hydrogen adsorption free energy (ΔG_H) of hydronium at the Mo-edge, being more favorable than that on the S-edge, as supported by density function theory (DFT) [38]. The electrons localized on the Mo-H bond are readily transferred to form dihydrogen, leading to improved catalytic performance. After the report of Jaramillo and co-workers in 2007 on the effectiveness of Mo-edge (2H phase), it was found that the Mo-edge is catalytically more active [supported on Au (111) surface] than the surface [39]. Previously, MoS_2 was also grown on W-anchored graphene for HER applications [40]. In other reports, N, S-carbon dots (CDs), intercalated MoS_2/graphene [41], onion-like graphene-surrounded MoS_2 [42], and exfoliation/doping-processed MoS_2 [43] were also applied as HER catalysts. These reports demonstrate the potential of MoS_2 as an HER catalyst.

In this review, we aim to provide a comprehensive understanding of MoS_2 nanomaterials as electrocatalysts for HERs and as material for super-capacitor (SC) applications. The MoS_2 and MoS_2-based materials possess excellent electrochemical properties, which makes them suitable candidates for HER and SC applications. The SCs are the electrochemical devices which bridge the conventional capacitors and batteries. Thus, it would be of great significance to summarize the progress in MoS_2-based materials for HER and SC applications. This work summarizes the previous development in the modification strategies of MoS_2, including increasing the interlayer spacing, phase transition, introducing sulfur vacancies, doping with various elements, and constructing a heterostructure with materials such as reduced graphene oxide (rGO), carbon nanotubes (CNTs), polymers, metal oxides, and MXenes. Finally, we will discuss the challenges and future direction of the development of high-performance MoS_2 catalysts for scalable and economical hydrogen production and energy storage applications.

2. MoS_2-Based Materials in Hydrogen Evolution Reactions (HERs)

MoS_2 has emerged as a promising catalyst to replace Pt-based electrocatalysts for HERs in water electrolysis due its unique layered structure, tunable electronic properties, abundance, low cost, and excellent catalytic potential and stability. However, its intrinsic HER performance is lower than that of Pt electrodes. To address this, various modifications have been dedicated to improving its HER activity, as will be discussed. A fundamental understanding of the water electrolysis mechanism is crucial. Water electrolysis consists of two half-cell reactions, where the HER takes place at the cathode and the OER takes place at the anode, as illustrated in Figure 2. To achieve efficient water splitting, appropriate catalysts are typically applied to the cathode and anode.

Figure 3 depicts the typical polarization curves for HERs, OERs, and their respective reactions at the cathode and anode. In addition to coating catalysts on the cathode or anode, the initiation of a water splitting reaction requires overcoming a free energy (ΔG) of 237.2 kJ mol^{-1} at 25 °C and 1 atm, irrespective of whether the medium is acid, alkaline, or neutral. This energy corresponds to a theoretical cell voltage of 1.23 V.

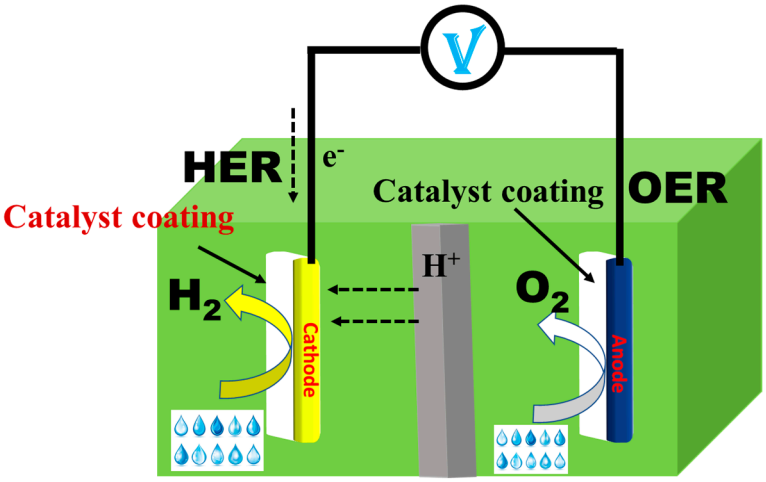

Figure 2. Schematic illustration of electrocatalytic water splitting for the H_2 and O_2 production.

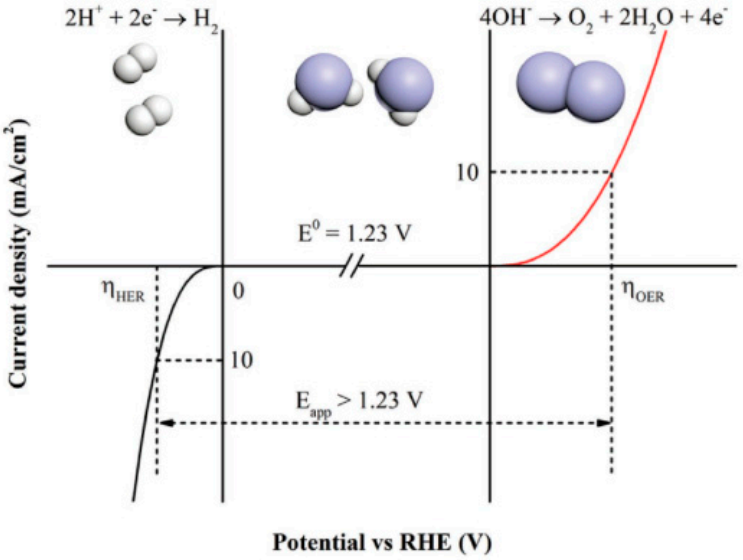

Figure 3. Schematic illustration of typical polarization curves for HERs and OERs and corresponding half-reactions. Reproduced with permission from Ref. [30], copyright, 2017, WILEY-VCH.

The HER is a half-cell reaction that occurs at the cathode during electrocatalytic water splitting, producing one molecule of H_2 through a two-electron transfer process. In an acidic medium, the HER involves three elementary reactions, as described by Equations (1)–(3). The first step is the Volmer reaction, in which protons are discharged onto the electrode surface, forming the adsorbed hydrogen intermediate (H_{ads}). This step represents the reduction in protons on the catalyst surface. This process is also analyzed through the Tafel slopes obtained from the experimental plots of the overpotential versus logarithm of the current density (mA cm^{-2}) [44,45].

$$\text{Volmer reaction: } H_3O^+ + e^- \rightarrow H_2O + H_{ads} \quad (1)$$

The second step is the electrochemical desorption, which can take place either via the Heyrovsky reaction or the Tafel reaction, depending on the surface coverage of the adsorbed hydrogen (H_{ads}).

$$\text{Heyrovsky reaction: } H_{ads} + H_3O^+ + e^- \rightarrow H_2O + H_2 \quad (2)$$

(when H_{ads} coverage is low);

$$\text{Tafel reaction: } H_{ads} + H_{ads} \rightarrow H_2 \quad (3)$$

(when H_{ads} coverage is high).

The mechanism of the HER can also be identified from the experimental values from the Tafel slope. For example, a Tafel value of 120 mV dec^{-1} indicates a Vomer step. On the other hand, Tafel slops of 40 and 30 mV dec^{-1} correspond to the Heyrovsky and Tafel steps, respectively, whereas in the case of alkaline and neutral electrolyte solutions, the H_{ads} in the HER process primarily originates from H_2O molecules. The adsorbed hydrogen intermediate (H_{ads}) plays a key role in the HER, irrespective of the pathway it follows. As a result, the free energy of hydrogen adsorption (ΔG_{Hads}) is widely regarded as a critical descripted for HER electrocatalysts. ΔG_{Hads} serves as an indicator of catalytic efficiency, reflecting the catalyst's ability to absorb and desorb H_{ads} effectively. Theoretical analysis suggests that electrocatalysts achieve optimal HER performance when the value of ΔG_{Hads} is close to zero [46]. This relationship can be visualized in a Volcano plot, as shown in Figure 4. In this plot, noble metals such as Pt exhibit ΔG_{Hads} values nearly close to zero, reflecting their highest HER electrocatalytic activity [47]. Moreover, changes in the electronic structure of a catalyst can significantly influence the adsorption behavior of intermediate hydrogen (H_{ads}) and its binding energy, thereby improving hydrogen production [48]. For example, upon forming transition–metal–metalloid compounds, such as MoS_2, the transition metal may occupy a new electronic environment [49]. This results in enhanced catalytic activity, as MoS_2 appears higher on the Volcano plot compared to Mo alone (Figure 4) [50]. While the inherent structure of bulk MoS_2 satisfied the basic requirement for HER applications, it often fails to deliver the desired electrocatalytic performance. Consequently, various strategies have been developed to improve its electronic properties and catalytic activity.

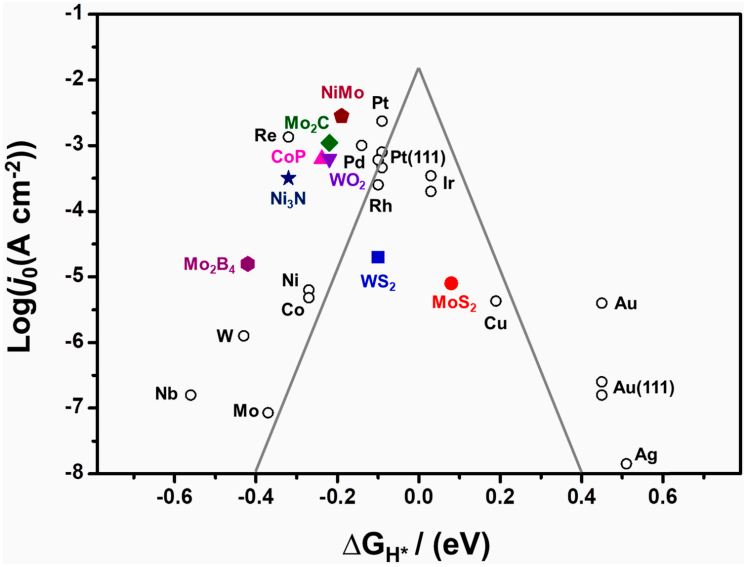

Figure 4. HER Volcano plot of the relationship of the exchange current density of certain metals and MoS_2 and their corresponding ΔG_{H^*}. Reproduced with permission from Ref. [46], copyright 2019, Elsevier.

Ultrathin materials, compared to their bulk materials, demonstrate significantly controlled charge transfers within each layer. Thus, the electronic structure of these materials can be finely tuned by reducing their thickness to an atomic scale. DFT calculations reveal ultrathin nanosheets possessing a significantly higher density of electronic states near the Fermi level compared to bulk materials [51]. This results in improved electron transfer

and conductivity, enhancing their performance in the water electrolysis process. In 2005, Novoselov et al. [52] conducted groundbreaking research by using the micromechanical cleavage method to extract the individual atomic planes of MoS_2 from its bulk form. Since then, substantial advancements have been made in the synthesis of single- or multilayer MoS_2 nanosheets. This reduction in thickness can transform the indirect band gap of bulk MoS_2 into a direct band gap, significantly boosting it efficiency for electrocatalytic hydrogen production [53]. Lukowaki et al. [54] utilized a chemical exfoliation method to convert the semiconducting 2H MoS_2 nanostructure into a metallic 1T MoS_2 phase. They found that nanosheets of the metallic MoS_2 polymorph exhibited significantly higher HER activity.

The HER activity of catalysts can be improved by regulating their active sites, which can be achieved by expanding the interlayer spacing of bulk MoS_2. Increasing the interlayer spacing provides more active sites, facilitates the desorption of H_{ads}, and improves the transfer of electrons/protons [55]. Moreover, this expansion optimized the ΔG_{Hads} at both the edge and the basal planes of MoS_2, facilitating intermediate H_{ads} adsorption and hydrogen molecule desorption, thereby boosting HER efficiency [56]. Zhang et al. [57] reported the design of 1T MoS_2 with expanded interlayer spacing using a simple solvothermal approach in N,N-dimethylformamide (DMF) derived from Mo-based organic frameworks (Mo-MOFs). The resulting 1T-MoS_2 demonstrated efficient HER activity, achieving an overpotential of 98 mV at a current of 10 mA cm^{-2}, along with a Tafel slope of 52 mV dec^{-1}. Hu et al. [58] synthesized a 1T/2H-MoS_2 material with an expanded interlayer spacing of 0.94 nm under reaction conditions of 200 °C in ethylene glycol (Figure 5a). This interlayer expansion was attributed to the incorporation of ammonium ions during the reaction, which creates large channels for ion transport and enhances the exposure of active sites. The resulting 1T/2H-MoS_2/NH^{4+}-200 demonstrated outstating HER performance, achieving an overpotential of 159.9 mV at 10 mA cm^{-2}, with a Tafel slope of 55.5 mV dec^{-1} in 0.5 M H_2SO_4 (Figure 5b,c). Moreover, the material demonstrated remarkable electrochemical stability, showing only a minor drop overpotential (7.2 mV) at 10 mA cm^{-2} after 1000 cyclic voltammetry cycles.

Heteroatom doping is a highly effective strategy to modify the electronic structure of the original lattice, reduce the hydrogen adsorption free energy (ΔG_{H^*}), activate the basal plane of MoS_2, and enhance its catalytic activity [59,60]. Additionally, doping with atoms of varying radii and valance electrons significantly alter the electron density of Mo and S atoms, increasing the electron transfer rate and conductivity, which further boosts the HER activity of MoS_2 [61,62]. Xie and co-workers [63] proposed a novel strategy to synthesized V-doped MoS_2 using semi-metallic interlayer doping. They reported that vanadium doping alters the electronic structure of MoS_2, facilitating the activation of valance electrons, shortening the electron pathways, and enhancing electrical conductivity and carrier concentration, thereby significantly improving the catalytic performance of MoS_2. Additionally, V doping reduced the band gap of MoS_2 due to interactions between the V atoms and neighboring Mo atoms. Zhao and co-workers [64] reported a covalent doping strategy to incorporate cobalt into MoS_2, creating a bifunctional electrocatalyst for overall water splitting (both HERs and OERs). The synthesized Co-MoS_2 catalyst demonstrated superior HER performances, with an onset potential of −0.02 V (vs. reversible hydrogen electrode (RHE) in 0.1 M KOH. The improved HER activity was attributed to cobalt doping, which effectively reduced the band gap of MoS_2 from 1.70 eV to 0 eV, thereby significantly improving its conductivity.

Single-atom catalysts represent a frontier in the field catalysis, gaining significant attention for their maximum atomic efficiency and tunable electronic properties. Li and co-workers [65] applied a novel single-atom catalysis approach to developed a highly active electrocatalyst with superior HER performance across a wide pH range. Initially, 2H-MoS_2

was synthesized using a simple two-step hydrothermal approach. Subsequently, different amounts of noble Ru metal were incorporated into 2H-MoS_2, as illustrated in Figure 6.

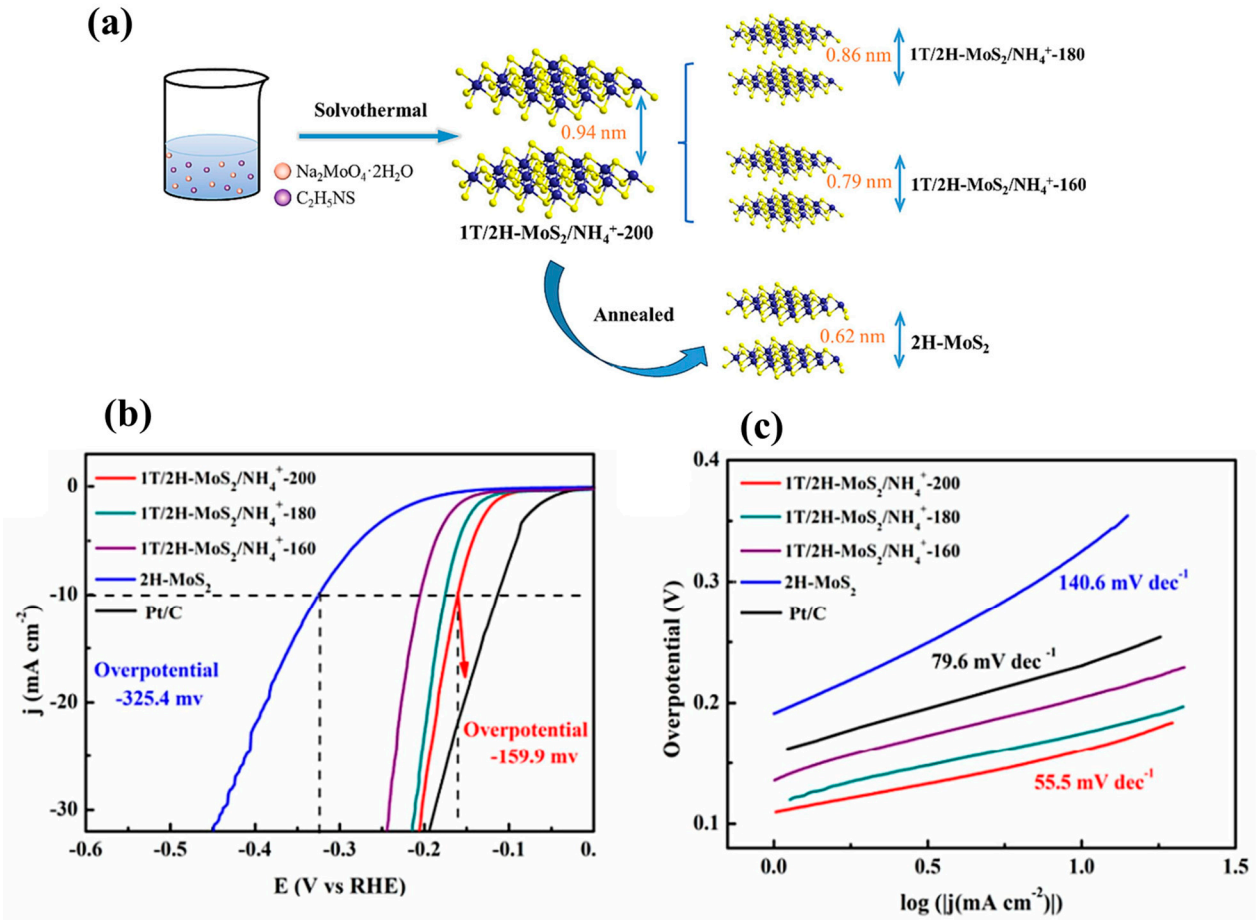

Figure 5. (**a**) Schematic presentation for the synthesis of 1T/2H-MoS_2 electrocatalysts with ammonium ions at different temperatures, (**b**) polarization, and (**c**) corresponding Tafel slopes of 1T/2H-MoS_2 electrocatalysts with ammonium ions at different temperatures at a 5 mV/S scan rate in 0.5 M H_2SO_4. Reproduced with permission from Ref. [58], copyright 2023, Elsevier.

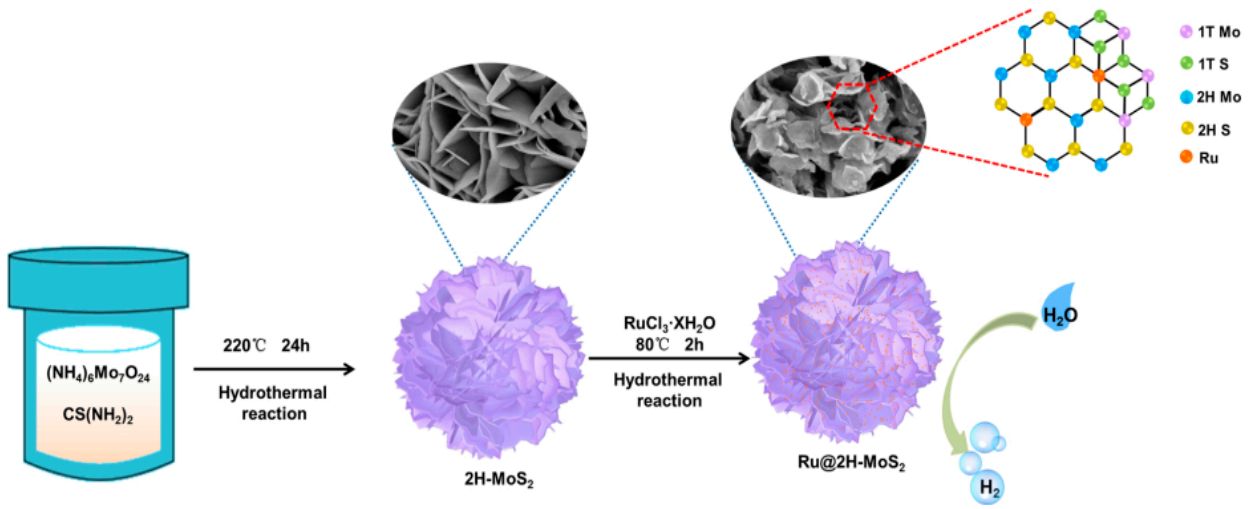

Figure 6. Schematic illustration for the synthesis of Ru single-atom-doped MoS_2 catalysts for HER applications. Reproduced with permission from Ref. [65], copyright 2021, Elsevier.

The decoration of Ru as a single atom was confirmed through HAAD-STEM analysis, where the bright spot in yellow circles confirmed the position of Ru single atoms in the 1T/2H-MoS_2 catalyst, as shown in Figure 7a–c. To further validate the presence of Ru single atoms in MoS_2, energy dispersive spectrometer (EDS) analysis was conducted, indicating the presence of Ru, Mo, and S atoms in the $Ru_{0.10}$@2H-MoS_2 catalyst (Figure 7d–g).

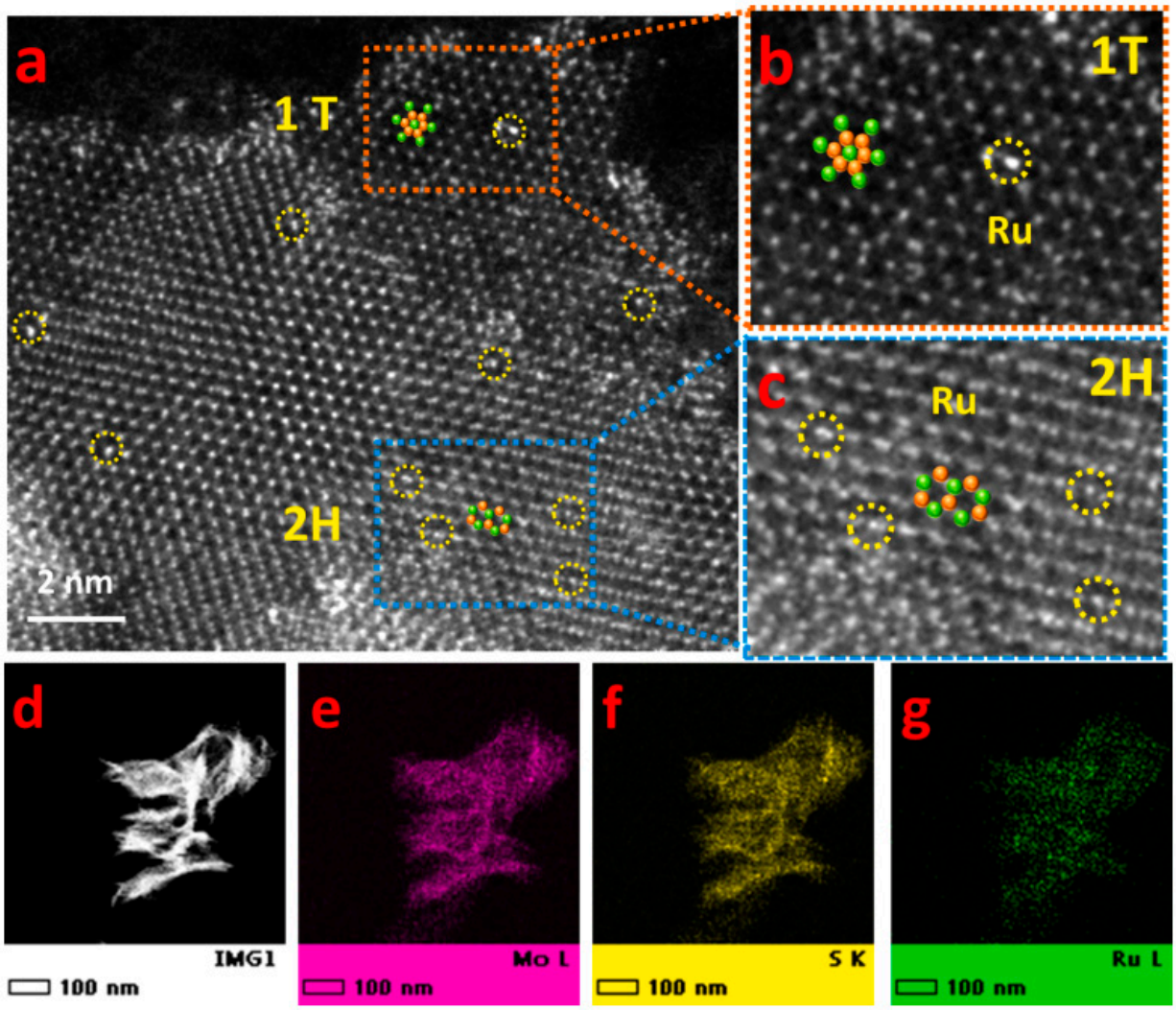

Figure 7. HAADF-STEM image of (**a**) optimized $Ru_{0.10}$@2H-MoS_2, (**b**,**c**) high resolution images of 1T and 2H phases decorated with Ru single atoms (marked by yellow circles), (**d**–**g**) EDS elemental mapping image of optimized $Ru_{0.10}$@2H-MoS_2 catalysts indicating the presence of Ru, Mo, and S atoms. Reproduced with permission from Ref. [65], copyright 2021, Elsevier.

The optimized $Ru_{0.10}$@2H-MoS_2 catalyst exhibited the highest HER activity, with the lowest overpotential of 137 mV at a current of 10 $mAcm^{-2}$ in 1.0 M PBS at pH 7, as shown in Figure 8a. The corresponding Tafel slope, as shown in Figure 8b, indicates a smaller slope compared to other catalysts, although a slightly higher one than that of commercial Pt/C. The electrochemical double-layer capacitance in Figure 8c demonstrates that $Ru_{0.10}$@2H-MoS_2 has better HER activity and improved charge transfer. Moreover, the charge transfer resistance of the optimized $Ru_{0.10}$@2H-MoS_2 is lower than that of other catalysts, further confirming that it has a faster HER reaction speed (Figure 8d). The incorporation of Ru single atoms in MoS_2 significantly reduces the ΔG_H of 2H-MoS_2, as confirmed by the DFT calculation.

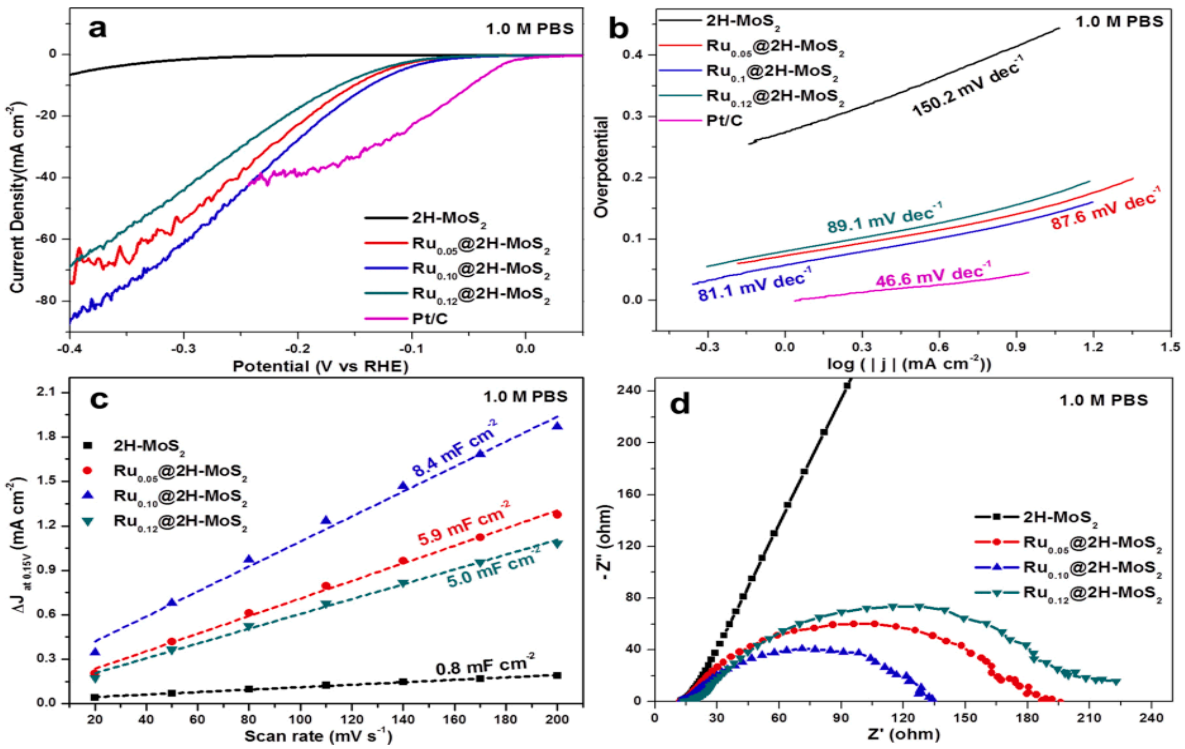

Figure 8. HER performance of Ru@2H-MoS_2 catalysts with varying loadings of Ru in 1.0 M PBS solution at pH 7, (**a**) polarization curves (**b**) corresponding Tafel slopes, (**c**) the electrochemical double-layer capacitance (C_{dl}), and (**d**) electrochemical impedance spectroscopy (EIS). Reproduced with permission from Ref. [65], copyright 2021, Elsevier.

The heterostructure coupling of two or more components is a highly efficient approach to modulate the interfacial electronic structure and improve the electrical conductivity of the base materials. This approach enhances the interfacial charge transfer, leading to improved catalytic performance [66,67]. Additionally, heterostructures create electrochemically active interfaces that enhance electrochemical properties and optimize the Gibbs free energy for hydrogen adsorption (ΔG_H) driven by synergistic effects at the interface [68,69]. To improve the electrical conductivity of MoS_2, Song and co-workers [70] developed a heterostructure with single-walled carbon nanotubes (SWNT). Their study revealed that electrons migrate from the SWCT to MoS_2 and accumulate around the S atom in MoS_2 within the MoS_2/SWNT heterostructure. This process resulted in the formation of an electrochemically active interface. Consequently, the MoS_2/SWNT heterostructure exhibited excellent hydrogen atom recombination and H_2 gas release, significantly improving HER performance due to the altered electronic structure induced by the electron transfer. Li et al. [71] designed a well-defined three-dimensional MoS_2/rGO heterostructure using a facile hydrothermal approach. DFT simulations revealed that graphene possesses stronger electron affinity than n-type MoS_2, as shown in Figure 9a–d. Following the formation of the active interface, electrons are initially transferred from MoS_2 to graphene due to the higher work function of MoS_2. This transfer causes MoS_2 to acquire a positive charge and graphene to acquire a negative charge through an electrostatic interaction. Once equilibrium is achieved at the Fermi level between MoS_2 and rGO, a built-in electric field forms, directed from MoS_2 to graphene. This field facilities rapid electron transfer from the electrode to graphene and subsequently to MoS_2 during electrolysis, as shown in Figure 9e,f.

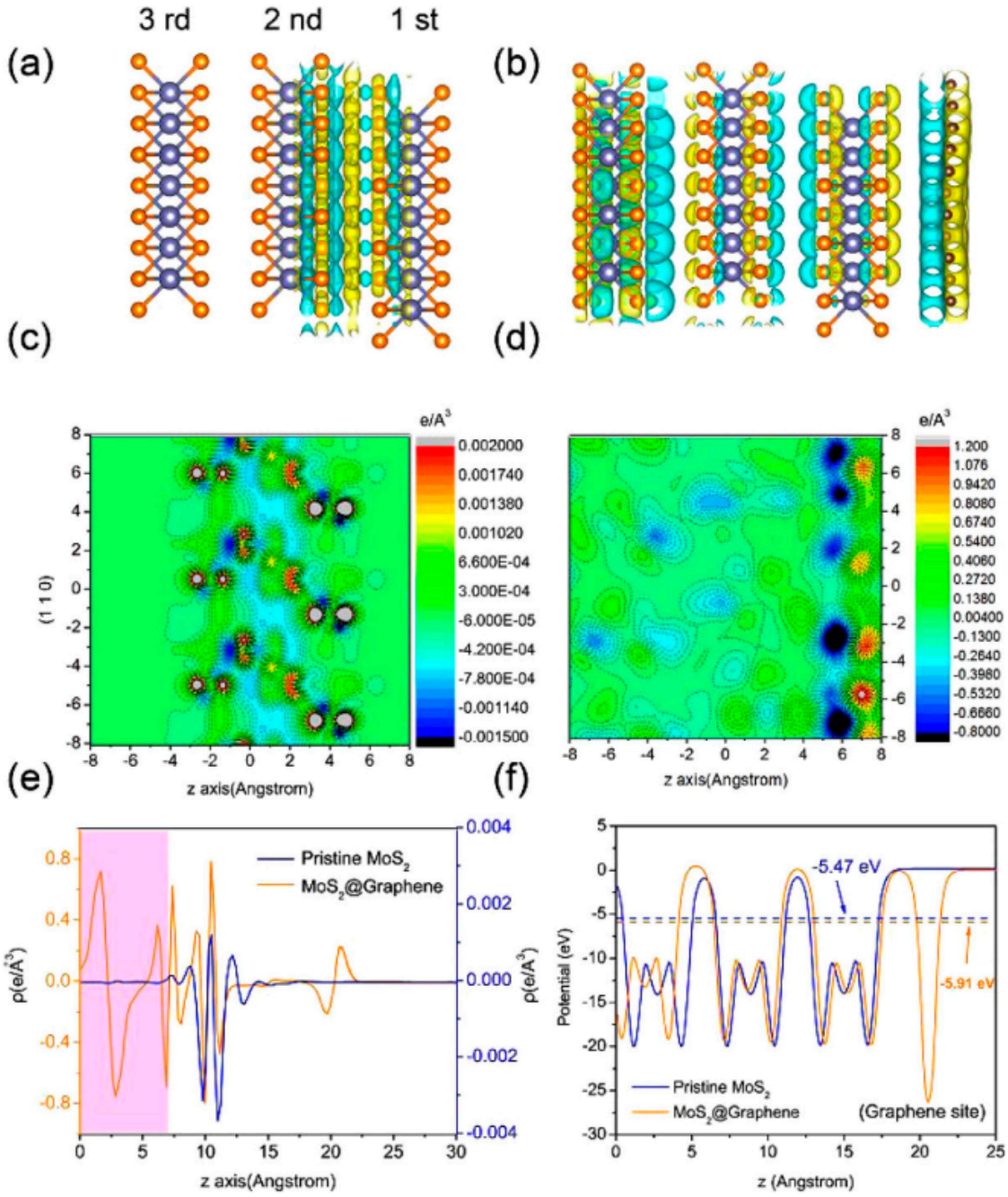

Figure 9. Charge density difference between (**a**) pristine MoS_2 and (**b**) MoS_2/graphene heterostructure. Blue color indicates depletion space and yellow color indicates accumulation space. (**c**,**d**) Plot of (110) surfaces of the charge density difference contour for pristine MoS_2 and MoS_2/graphene, (**e**) x-y plane averaged charge density, with charge density on the *y*-axis and distance along *z*-direction on the *x*-axis. (**f**) Average electrostatic potential of pristine MoS_2 and MoS_2/graphene. Reproduced with permission from Ref. [71], copyright 2015, Nature.

The formation of an electrochemically active interface rearranges and optimizes electron transfer pathways, enhances the conductivity of MoS_2, and improves its adsorption energy, collectively leading to a superior catalytic performance (Figure 10a,b).

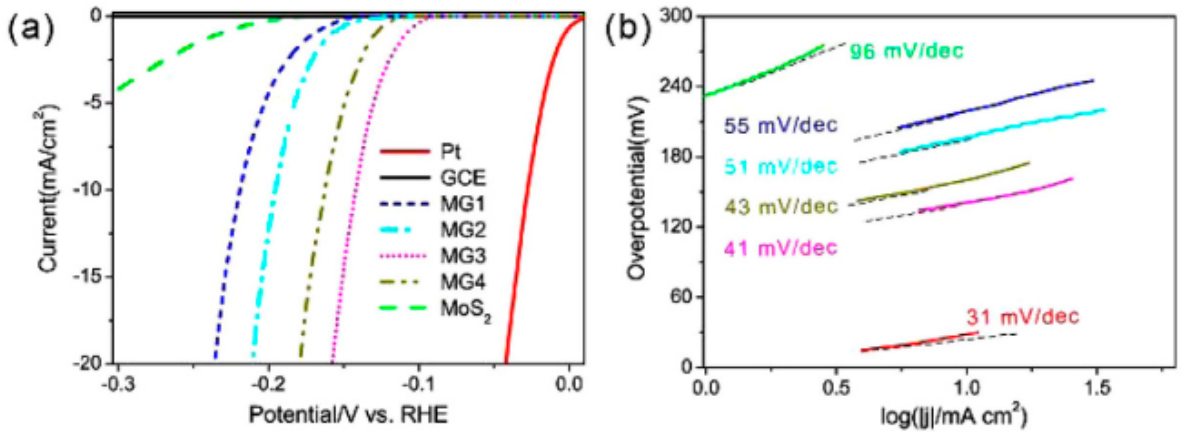

Figure 10. (**a**) Polarization curves obtained for pristine MoS_2 and MoS_2/graphene heterostructure at 140, 160, 180, and 200 °C (denoted MG1–4), and (**b**) corresponding Tafel plots. Reproduced with permission from Ref. [71], copyright 2015, Nature.

Liu et al. [72] synthesized a $MoO_2/MoS_2/C$ hollow nanoreactor with a monodispersed sandwich structure and a unique triple-layer "conductor/catalyst/protector" configuration. The design effectively enhances the HER performance across all pH values. The metallic MoO_2 substrate, known for its ultrahigh intrinsic conductivity, facilitates rapid charge transfer, whereas sulfur vacancies were introduced to activate the highly exposed (002) facets of MoS_2, enhancing catalytic activity. The optimized $MoO_2/MoS_2/C$ hollow nanoreactor achieved overpotentials of 77, 91, and 97 mV at a current of 10 mA in acidic, alkaline, and neutral media, respectively, with corresponding Tafel slopes at 41, 49, and 53 mV dec^{-1}, demonstrating its excellent catalytic efficiency. Fu et al. [73] developed an ultrathin $MoS_2/g\text{-}C_3N_4$ heterostructure using an in situ interfacial engineering approach. The synthesized $MoS_2/g\text{-}C_3N_4$ heterostructure demonstrated outstanding HER performance, with overpotential and Tafel slope values comparable to that of commercial Pt catalysts. The excellent HER activity was attributed to van der Waal interactions and the strong interfacial coupling via Mo-N bonds, which significantly enhanced the hydrogen adsorption and reduction kinetics, thereby boosting overall HER efficiency. Chen et al. [74] dementated the design of a $1T\text{-}MoS_2/Ni(OH)_2$ heterostructure via an interface engineering strategy to achieve excellent HER activity. The optimized heterostructure exhibited superior HER performance in an alkaline electrolyte (1 M KOH), achieving a low overpotential of 57 mV at a current of 10 mA and a corresponding Tafel slope of 30 mV dec^{-1}, highlighting its excellent catalytic efficiency. Huang and colleagues [75] demonstrated a method for creating a high performance HER electrocatalyst by combining MoS_2 with Ni_2O_3H (MoS_2/Ni_2O_3H). Their strategy involved modifying the interface electronic structure to significantly improve the HER activity. The resulting heterostructure demonstrated excellent alanine HER activity, with a low overpotential of 84 mV at 10 mA cm^{-2} and a small charge transfer resistance of 1.5 Ω. Additionally, the catalyst exhibited outstanding long-term stability. DFT calculations revealed that the Ni 3d of Ni2O3H were significantly activated, serving as an electron depletion center to facilitate rapid electron transfer during HERs. Wu et al. [76] synthesized the MoS_2/Co_9S_8 heterostructure nanosheets on carbon cloth (MoS_2/Co_9S_8/CC) using a sulfurization method. This approach effectively enhanced the HER activity by leveraging the synergistic effects of the heterostructure and the conductive carbon cloth substrate. The synthesized MoS_2/Co_9S_8/CC catalyst was thoroughly analyzed to confirm its distribution and heterostructure formation. As shown in Figure 11a,b, the XRD pattern and Raman spectra confirm the successful synthesis of a MoS_2/Co_9S_8/CC heterostructure catalyst. Figure 11c,d show the scanning electron microscopic images of MoS_2/Co_9S_8/CC catalysts,

indicating that the heterostructure nanosheets were uniformly grown on carbon cloth. This growth formed a network-like structure, which is conductive to the improved electron transport and increased exposure of active sites. Transmission electron microscopy (TEM) revealed that MoS_2 nanosheets, consisting of 4–8 layers, were distributed on the surface of Co_9S_8, as shown in Figure 11e,f. The formation of a heterostructure between MoS_2 and Co_9S_8 was evident, with atomic-level connections that facilitate enhanced electron transfer due to the presence of additional boundary active sites in MoS_2. The lattice spacing was measured as 0.61 nm for the (002) planes of MoS_2 and 0.35 nm for the (220) planes of Co_9S_8 (Figure 11 g). The EDS elemental mapping results in the scanning transmission electron microscopy (STEM) mode further confirmed the uniform distribution of Co, Mo, and S elements (Figure 11g–k). The catalytic performance of developed MoS_2/Co_9S_8/CC catalysts was tested in a three-electrode electrochemical system using a 1 M KOH electrolyte. As shown in Figure 12a, the linear sweep voltammeter (LSV) curve of MoS_2/Co_9S_8/CC, Co_9S_8/CC, and MoS_2CC indicted an overpotential of 73 mV at a current density of 10 mA cm^{-2}, which is significantly lower than those of Co_9S_8/CC (199 mV), MoS_2/CC (157 mV), and CC (373 mV). The corresponding Tafel slope, shown in Figure 12b, revealed that MoS_2/Co_9S_8/CC has a much smaller Tafel slope of 78 mV dec^{-1} compared to other catalysts, indicating faster HER kinetics. These results demonstrated that the MoS_2/Co_9S_8/CC heterostructure significantly enhances HER activity.

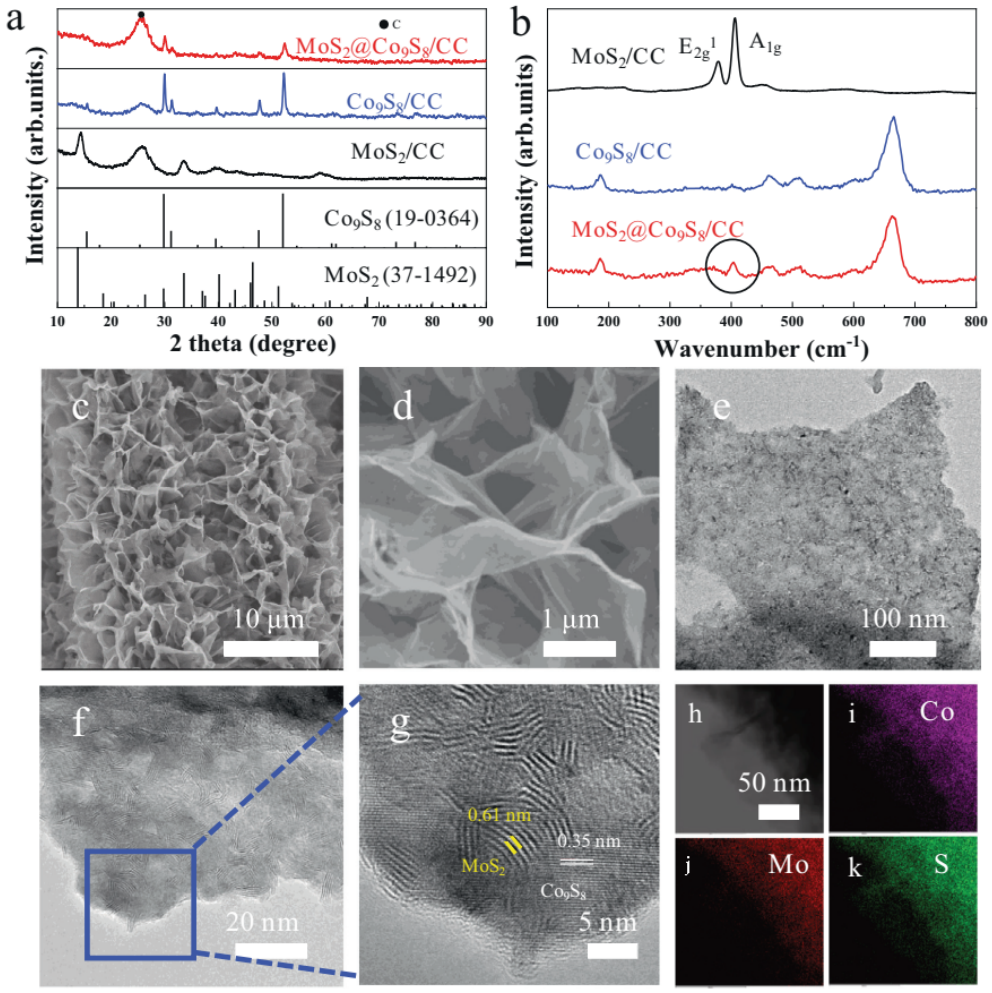

Figure 11. (**a**). XRD pattern and (**b**) Raman spectra of Co_9S_8, Co_9S_8/CC, MoS_2/CC, and Co_9S_8/MoS_2/CC; (**c**,**d**) SEM, (**e**,**f**) TEM, and (**g**) HRTEM images of Co_9S_8/MoS_2/CC at different magnifications; and (**h**) corresponding EDS mapping of (**i**–**k**) Co, Mo, and S. Reproduced with permission from Ref. [76], copyright 2021, Elsevier.

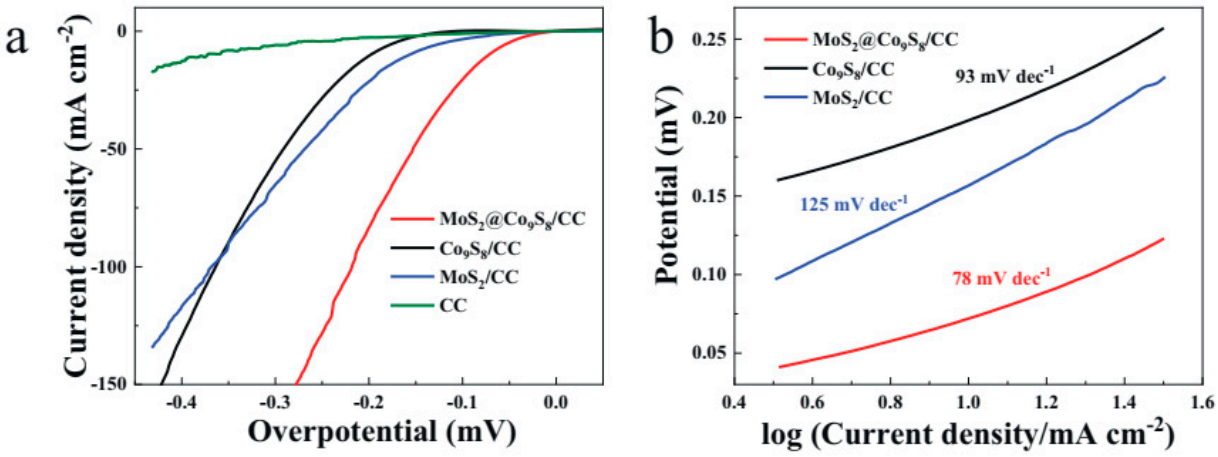

Figure 12. (**a**) HER polarization curves and (**b**) corresponding Tafel plots of synthesized pristine and composite catalysts (Co_9S_8/CC, MoS_2/CC, and Co_9S_8/MoS_2/CC). Reproduced with permission from Ref. [76], copyright 2021, Elsevier.

Table 1 shows the previous reports on MoS_2-based materials for HER applications [77–98].

Table 1. Electrochemical performance of MoS_2-based electrodes for HER applications.

Catalysts	Synthesis Method	Electrolyte	Stability	Overpotential (mV)	Tafel Slope (mV/dec)	Ref.
MoS_2-MoO_3-x/Ni_3S_2	Electrochemical/ electrodeposition	1.0 M KOH	17 h	76	53.2	[77]
3D-Co-MoS_2/G	Hydrothermal	0.5 M H_2SO_4	5000 Cycles	143	71	[78]
$MoS_2-CoS-Zn$	Solvothermal	0.5 M H_2SO_4	60 h	72.6	37.6	[79]
Ni_2P/MoS_2/N: RGO	Heating method	0.5 M H_2SO_4	3000 Cycles	39.5	39.52	[80]
$MoS_2/CoNi_2S_4$	Hydrothermal	1.0 M KOH	48 h	78	67	[81]
$NiFeO_x(OH)_y$@ MoS_2/rGO	Sol–gel	1.0 M KOH	12 h	170	80	[82]
$Co_9S_8-MoS_2$/NF	Hydrothermal	1.0 M KOH	60 h	167	81.7	[83]
MoS_2/NiCo/CC	Hydrothermal	0.5 M H_2SO_4	17 h	153	51.1	[84]
$Mo_6Te_6/MoS_{2(1-x)}Te_{2x}$	CVD	0.5 M H_2SO_4	1000 Cycles	320	55.7	[85]
MoS_2/MoP	Hydrothermal	1.0 M KOH	30 h	92	59.8	[86]
MoS_2/CoNi@G	Hydrothermal	0.5 M H_2SO_4	10,000 Cycles	150	66	[87]
MoS_2-MoP/NC	Hydrothermal	1.0 M KOH	10,000 Cycles	35	30	[88]
Co_9S_8@MoS_2/N-carbon	Calcination in argon	1.0 M KOH	12 h	126	74.1	[89]
CoS_2@MoS_2/CC	Hydrothermal	1.0 M KOH	5000 Cycles	31	39.4	[90]
NCT@CoP@ MoS_2	Pyrolysis method	1.0 M KOH	5000 Cycles	195	74	[91]
MoS_2-Ti_3C_2 MXene	Hydrothermal	0.5 M H_2SO_4	1000 Cycles	98	45	[92]
$MoS_2-Ti_3C_2T_x$-P	Solvothermal	0.5 M H_2SO_4	-	298	120	[93]
MoS_2 QDs/$Ti_3C_2T_x$	Solvothermal	0.5 M H_2SO_4	500 Cycles	220	72	[93]
Co-MoS_2/V_2C	Hydrothermal	1 M KOH	10,000 Cycles	70.1	98.6	[94]
MoS_2/Ti_3C_2@CNFs	CVD	0.5 M H_2SO_4	3000 Cycles	142	113	[95]
MoS_2/CoS_2-2@$Mo_2TiC_2T_x$	Hydrothermal	0.5 M H_2SO_4	1000 Cycles	80	108.3	[96]
MoS_2 QDs/MXene	Hydrothermal	0.5 M H_2SO_4	1000 Cycles	307	68.5	[97]
MoS_2/graphdiyne nanotube/MXene	Hydrothermal	0.5 M H_2SO_4	3000 Cycles	109	55	[98]

3. MoS_2-Based Materials for Energy Storage

3.1. MoS_2 as Electrode Material

MoS_2 possesses excellent electrochemical characteristics, which make it a promising electrode modifier for SCs. In this connection, Gupta et al. [99] reported a specific capaci-

tance (C_{sp}) of 205.41 F/g at a current density of 0.25 A/g. An electrode modifier (MoS_2) was synthesized using a hydrothermal method and was explored for the construction of working electrodes for SCs. This work indicated that MoS_2 is a suitable candidate for electrochemical energy storage devices. Joseph et al. [100] prepared 1 T-MoS_2/carbon microspheres (CMSs) using the hydrothermal method and applied them for the construction of an SC electrode. The constructed electrode exhibited a C_{sp} of 692 F/g at 1 A/g under a three-electrode assembly system. This work also achieved a high power density of 775 W/kg and a high energy density of 46 Wh/kg. Authors observed that the prepared electrode had a decent stability of up to 20,000 cycles. Varasteanu et al. [101] systematically investigated the electrochemical performance of the electrochemically co-deposited MoS_2 nanoflakes and poly-naphthalenemethylamine. The fabricated polymer/MoS_2 composite facilitates the charge transport and intercalation of the ions, and an improved C_{sp} of 130 mF/cm^3 was obtained at a scan rate of 5 mV/s. Lee et al. [102] reported a benign hydrothermal method for the preparation of novel oxygen (O)-incorporated MoS_2 with a 1T/2H hybrid phase on a graphite foil (GF) substrate. The preparation of the 1T/2H-O-MoS_2@GF can be seen in Figure 13. It was observed that the 1T/2H hybrid phase prepared by employing Mo-blue clusters simultaneously demonstrated excellent stability in the 2H phase and high electrical conductivity in the 1T phase. The 1T/2H-O-MoS_2@GF exhibited a Csp of 280 F/g at 1 A/g with a stability of 10,000 at 10 A/g.

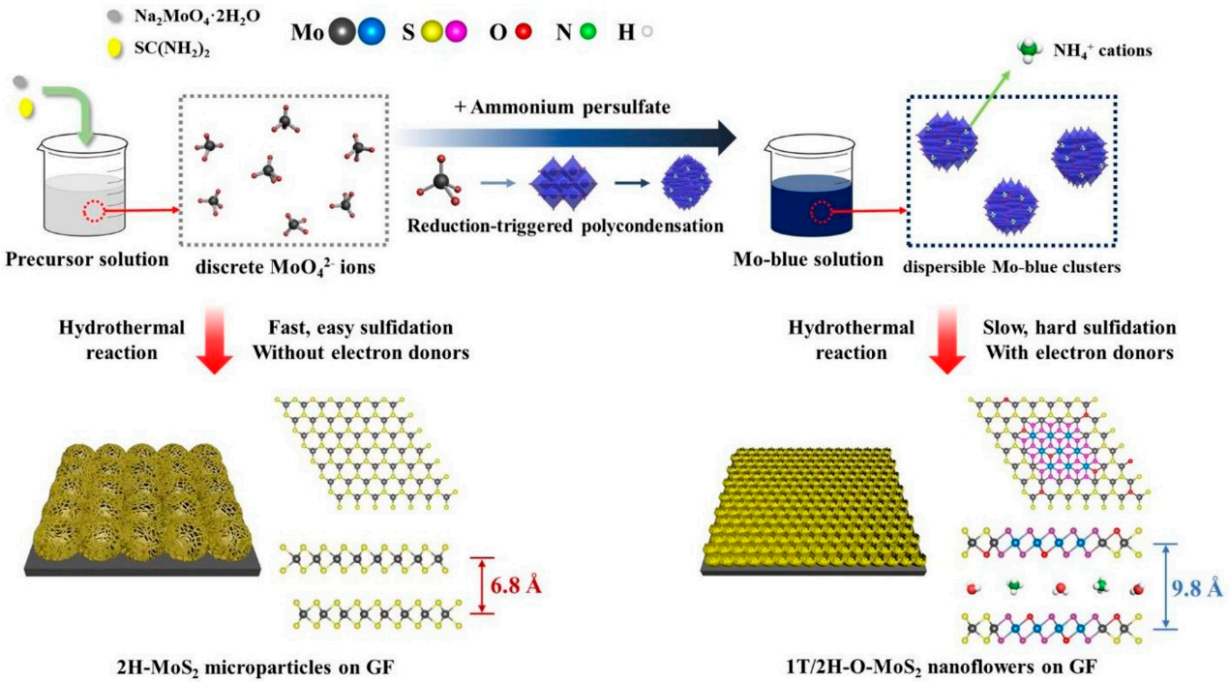

Figure 13. Pictorial illustration for the hydrothermal preparation of 2H-MoS_2 and 1T/2H-O-MoS_2 on GF. Reproduced with permission [102].

In another article [103], 2H-MoS_2 was fabricated using the hydrothermal method route and its electrochemical performance was studied as electrode modifier for the development of electrochemical devices. Authors obtained C_{sp} of 115.42 F/g at 10 mV/s and stability of 5000 cyclic voltammetry (CV) cycles. Kour et al. [104] also proposed the synthesis of mixed phase of 1T/2H MoS_2 as shown in Figure 14. It was believed that presence of synergistic effects in the prepared mixed phase of 1T/2H MoS_2 may exhibit better electrochemical properties. Authors used two different techniques, i.e., conventional hydrothermal (HT) and microwave assisted hydrothermal (MHT) methods for the preparation of electrode materials (1T/2H MoS_2). Authors used CV, electrochemical impedance spectroscopy (EIS)

and gravimetric charge–discharge (GCD) techniques to investigate the super capacitive performance of the prepared MS-HT and MS-MW samples. The MS-MW based electrode delivered C_{sp} of 421 F/g whereas MS-HT delivered C_{sp} of 742 F/g at 5 mV/s. The MS-HT based electrode also demonstrated excellent stability of 1200 cycles.

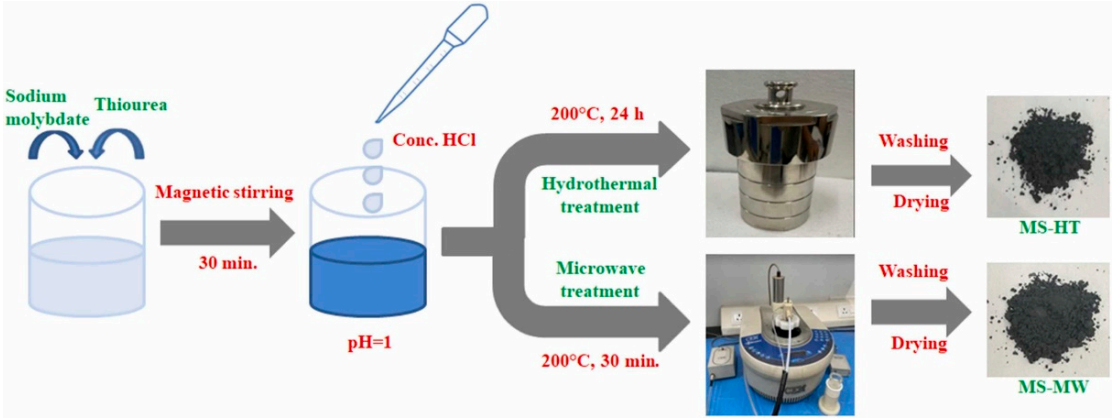

Figure 14. Schematic view for the synthesis of MS-HT and MS-MW samples. Reproduced with permission [104].

Teli et al. [105] electro-deposited MoS_2 on nickel foam (NF) and applied it as working electrode for SCs. A C_{sp} of 416.9 mF/cm^2 was obtained at 1 mAcm^{-2} in 1 M Na_2SO_4 electrolyte. According to Naz et al. [106], covalently functionalized 1T-MoS_2 (Fc-1T-MoS_2) nanoheets (NSs) exhibits decent electrochemical properties and C_{sp} of 501 F/g was achieved at 1 A/g with acceptable stability of 2000 cycles. Xu et al. [107] employed the hydrothermal method to prepare the multi-layered 1T-MoS_2 with high purity. The authors adopted the combination of sodium borohydride and ethanol to control the purity of the multi-layered 1T-MoS_2. The multi-layered 1T-MoS_2 shows a C_{sp} of 250.3 F/g at 1 A/g and an excellent stability of 5000 cycles.

3.2. Doped MoS_2 as Electrode Material

Doping with cobalt (Co) or manganese (Mn), etc., may improve the electrochemical properties of the MoS_2. Thus, Rohith et al. [108] employed Co as a dopant and MoS_2 as a host to fabricate the Co-doped MoS_2 as an electrode material for electrochemical energy storage applications. Authors achieved a C_{sp} of 86 F/g at 1 A/g for a two-electrode assembly system with excellent stability of 10,000 GCD cycles. Fayed et al. [109] proposed that nitrogen (N) and Co-doped MoS_2 may exhibit better electrochemical features and adopted a hydrothermal synthetic procedure for the preparation of the N and Co-doped MoS_2. The N and Co-doped MoS_2 shows a C_{sp} of 1400 F/g at 1 A/g. Asha and co-workers [110] have prepared MoS_2 and iron (Fe)-, nickel (Ni)-, and Co-doped MoS_2 on carbon cloth (CC) using the hydrothermal method. The synthesized materials were used for SC applications. The GCD curves of the MoS_2/CC and Ni-MoS_2/CC electrodes are shown in Figure 15a,b, respectively. It can be seen that the Ni-MoS_2/CC electrode exhibits better charge storage features compared to the MoS_2/CC electrode.

The GCD curves of the Fe-MoS_2-, MoS_2-, Co-MoS_2-, and Ni-MoS_2-based electrodes are displayed in Figure 15c. It was observed that the Ni-MoS_2-based electrode shows improved charge storage properties compared to the other electrodes at a current density of 1 A/g (Figure 15d). A decent C_{sp} of 305.9 F/g was obtained for the Ni-MoS_2/CC-based electrode, which is higher than MoS_2/CC (170.2 F/g). Authors also reported acceptable stability for 5000 cycles. In another report [111], manganese (Mn)-doped MoS_2 was prepared by the hydrothermal method for the preparation of working electrodes for SCs. The obtained

Mn-MoS_2 shows a C_{sp} of 430 F/g with a stability of 5000 cycles. Charapale et al. [112] also reported the fabrication of Fe-doped MoS_2 and achieved a C_{sp} of 545 F/g at 1 A/g with a cyclic stability of 2000 cycles. Khichi et al. [113] proposed the fabrication of novel $MoS_{2(1-x)}Se_{2x}$ (x = 0, 0.25, 0.5, 0.75, and 1) electrode materials, as demonstrated in Figure 16. This optimized MoS_1Se_1 electrode material shows excellent electrochemical properties and an improved C_{sp} of 266.51 F/g at 0.5 A/g. Authors also observed that the proposed electrode is stable up to 6000 cycles.

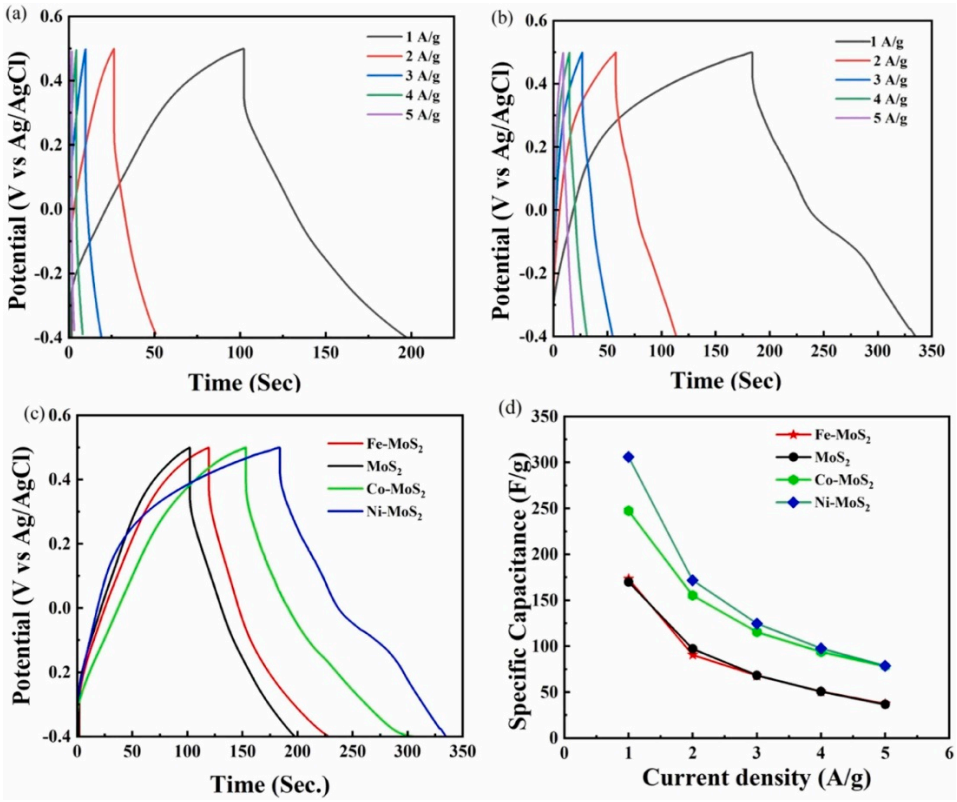

Figure 15. (**a**) GCD graphs of MoS_2/CC (**a**) and Ni-MoS_2/CC (**b**) at different current densities. GCD curves (**c**) and C_{sp} versus current density variations (**d**) of Fe-MoS_2-, MoS_2-, Co-MoS_2-, and Ni-MoS_2-based electrodes. Reproduced with permission [110].

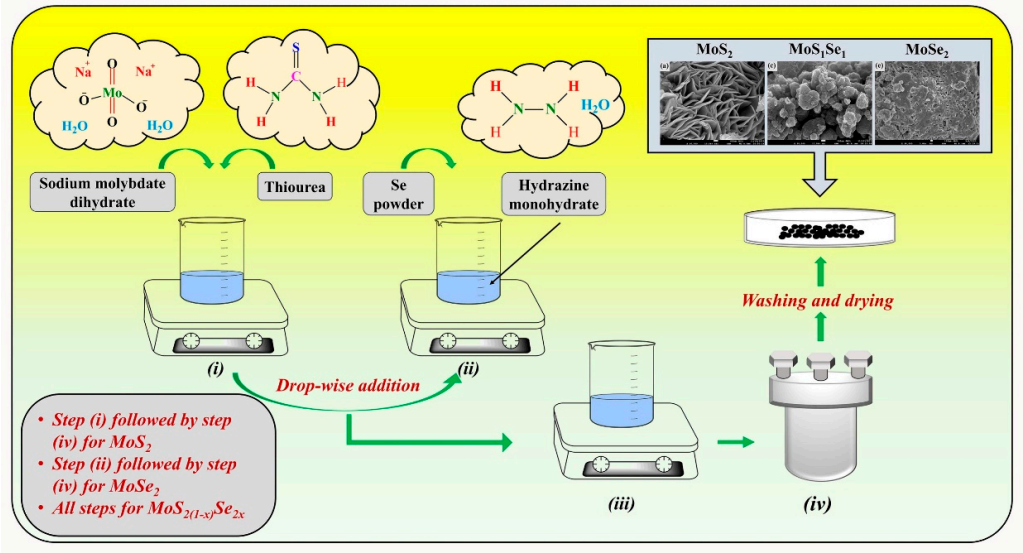

Figure 16. Schematic representation of the preparation of $MoS_{2(1-x)}Se_{2x}$ (x = 0, 0.25, 0.5, 0.75, and 1). Reproduced with permission [113].

3.3. MoS_2-Based Hybrid Materials as Electrode Material

According to Zhang et al. [114], the MnO_2/MoS_2-based electrode showed a C_{sp} of 224 mF cm^{-2} with a cyclic stability of 3000 cycles. In another work [115], a MoS_2-RuO_2 composite was prepared using a facile hydrothermal-assisted chemical reduction approach followed by calcination. The prepared hybrid material showed a C_{sp} of 972 F/g at 1 A/g with a decent stability of 10,000 cycles. A tin oxide-modified MoS_2 (SnO_2/MoS_2)-based electrode showed a C_{sp} of 567 F/g at 2 mV/s [116]. In another report [117], a SnO_2-MoS_2-based electrode exhibited a decent C_{sp} of 415 F/g at 1 A/g. This may be ascribed to the synergistic interactions between the SnO_2 and MoS_2. MoS_2 was also modified with SnO_2 quantum dots (SQD) to further investigate the effects of SQD for energy storage applications [118]. The proposed electrode material shows a C_{sp} value of 505 F/g at 1 A/g and a cyclic stability of 5000 cycles at 10 A/g. This interesting performance may be attributed to the structural integrity, high conductivity, and better electron electrochemical reactivity of the prepared electrode. Iqbal et al. [119] reported the hydrothermal preparation of a MoS_2@TiO_2 composite and explored it as an electrode material for SCs. The investigations showed that the MoS_2@TiO_2 composite has a decent Csp of 210 F/g at 10 mV/s with an acceptable cyclic stability of 2000 cycles. Ma et al. [120] grew a zinc sulfide (ZnS)/MoS_2 hybrid composite material on Mo foil via the hydrothermal method. The prepared electrode showed a Csp of 956.3 F/g at 10 mA/cm^2 and a long-term stability of 2000 cycles. Liu et al. [121] reported the novel electrode material of nickel sulfide (NiS_2)/MoS_2 on NF using an in situ hydrothermal method. This electrode demonstrated a Csp of 4.46 F/cm^3 at 5 mA/cm^2 and an acceptable cyclic stability of 3000 cycles. An iron sulfide (FeS_2)/MoS_2-based electrode revealed the presence of high conductivity and synergistic interactions [122]. A FeS_2/MoS_2-based electrode showed a C_{sp} of 495 mF/cm^2, which is higher than that of pristine MoS_2 (132 mF/cm^2) and FeS_2 (315 mF/cm^2) at 1 mA/cm^2. Authors also stated that the proposed electrode material has a decent cyclic stability of 5000 cycles. In 2020, a nickel molybdenum oxide ($NiMoO_4$)@MoS_2 core–shell structure was prepared using a two-step hydrothermal method [123]. The presence of synergism in the prepared hybrid electrode material lead to the generation of a high C_{sp} of 2246.7 F/g with 5000 cycles. Wu et al. [124] reported the fabrication of three-dimensional (3D) flower bud-like phosphorus (P) and tungsten (W) co-doped nickel cobalt sulfide ($NiCo_2S_4$)/MoS_2 composites (P, W-NCS@MS) via the hydrothermal method (Figure 17). The synthesized P, W-NCS@MS was explored as an electrode modifier, which demonstrated a Csp of 1250 C/g at 1 A/g with a stability of 10,000 cycles.

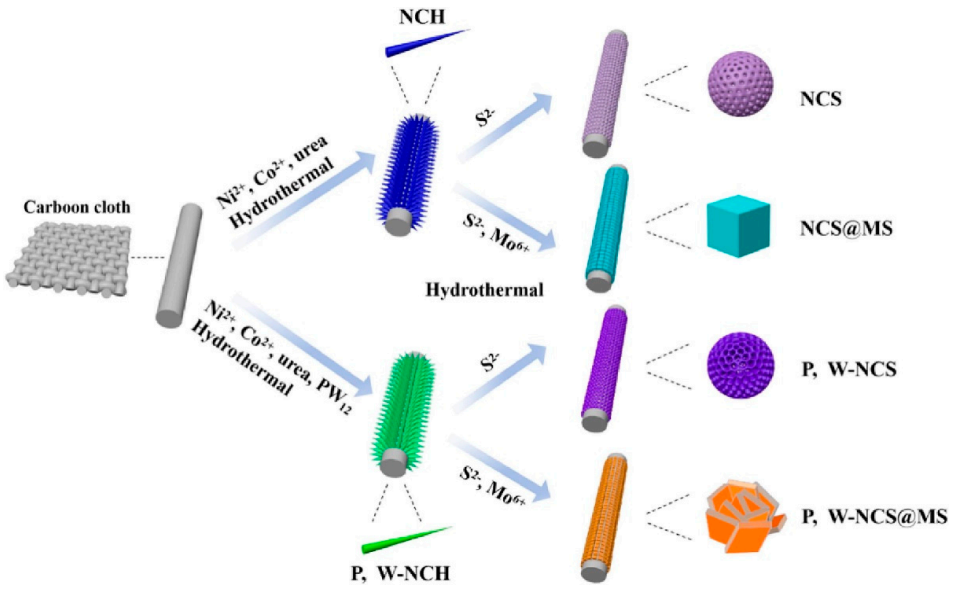

Figure 17. Schematic graph shows the synthetic protocols. Reproduced with permission [124].

3.4. MoS_2/Carbon-Based Composites as Electrode Material

In another article [125], single-layered MoS_2/graphene NSs were fabricated on activated carbon nanofibers (MoS_2@G/AC) using an electrospinning process. The prepared electrode material exhibited a high specific surface area of 850.2 m^2/g with a diameter of around 100 nm. Authors found that 0.5 MoS_2@G/AC had a high C_{sp} of 334 F/g at 0.5 A/g and, contrastingly, of 246.3 F/g at 10 A/g (electrolyte 3 M KOH). The 0.5 MoS_2@G/AC also retained excellent stability of 5000 cycles with a retention of 83.8%. Authors believed that the improved electrochemical activity of the electrode may be ascribed to the high surface area, promising pore structure, and synergistic interactions between the three components. A C_{sp} of 13.6 mF/cm^2 and cyclic stability of 1000 cycles were reported for the MoS_2/electrochemically exfoliated graphene (EEG)-based electrode [126]. The MoS_2/rGO composite also showed a C_{sp} of 460 F/g at 1 A/g with a decent cyclic stability of 5000 cycles [127]. In another article [128], a flake-like MoS_2/r-GO composite-based electrode exhibited a C_{sp} of 441 F/g at 1 A/g and a cyclic stability of 1000 cycles at 80 mV/s.

It is well known that mixed-phase MoS_2 has impressive electrochemical properties, which originate from the generation of electrochemical active sites and higher structural stability compared to the other materials with a crystalline nature. In this connection, Bokhari et al. [129] reported the one-pot synthesis of N-doped, rGO-modified, mixed-phase (MP) MoS_2 nanoflowers (NGM). The preparation of the electrode material can be seen in Figure 18. The NGM composite-based electrode exhibited a Csp of 539.5 F/g and a power density of 25.4 kW/kg. It was stated that the robust ion transport and low charge transfer resistance at the electrode–electrolyte interface may boost the electrochemical charge storage properties of the NGM-based electrode.

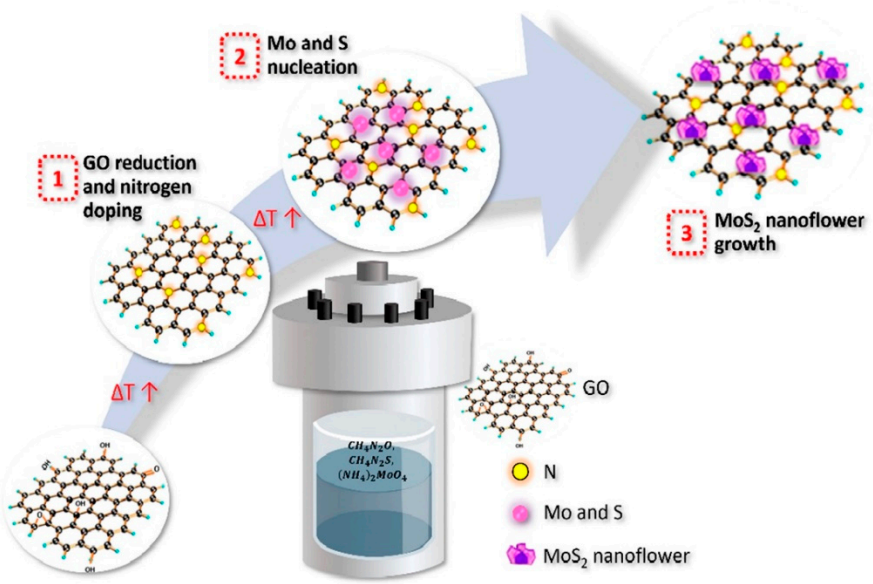

Figure 18. Schematic view of the preparation of the electrode material. Reproduced with permission [129].

Wang et al. [130] obtained a C_{sp} of 392 F/g at 5 mV/s using a hydrothermally prepared MoS_2/graphene composite modified electrode. Authors also obtained a C_{sp} of 76 F/g at 5 mV/s for a 2D printing-based fabrication process using MoS_2/graphene ink. Pilathottathil et al. [131] prepared AC/MoS_2, graphene/MoS_2, and MWCNTs/MoS_2 using benign approaches. The fabrication of SC devices are demonstrated in Figure 19. Authors observed that AC/MoS_2 has superior electrochemical properties and exhibited a decent C_{sp} of 216 F/g with an energy density of 6.2 Wh/kg. In contrast, graphene/MoS_2 showed a C_{sp} of 202 F/g, whereas MWCNTs/MoS_2 exhibited a C_{sp} of 161 F/g.

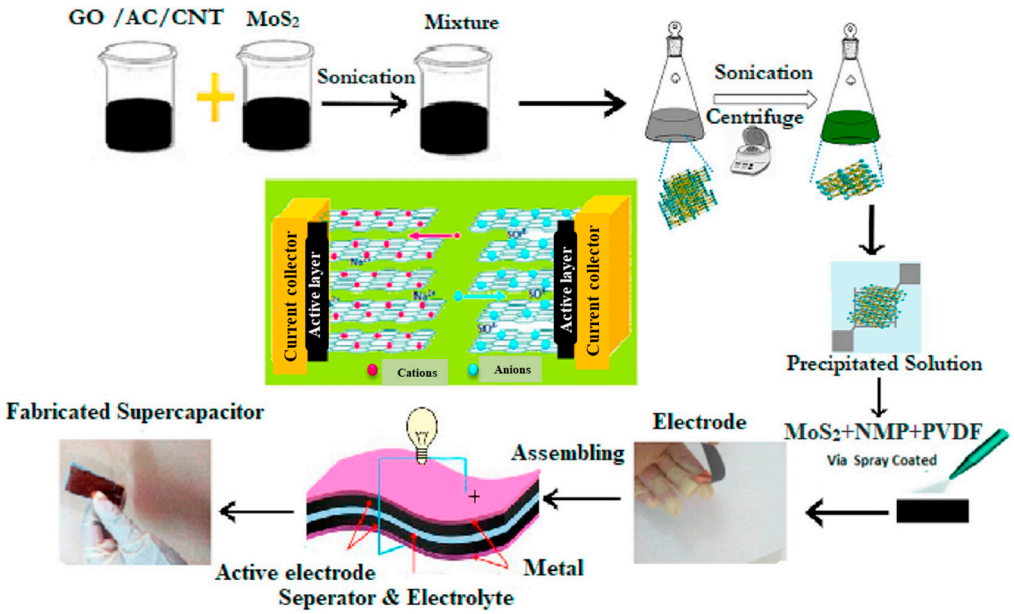

Figure 19. Schematic graph shows the synthesis and fabrication of SCs. Reproduced with permission [131].

Kour et al. [132] used mixed-phase MoS_2 anchored carbon nanofibers (CNFs) by employing the hydrothermal route. Authors prepared a series of MS/CNF_{-x} composites (where x = 1, 1.5, 2, and 3) to optimize the electrochemical performance of the proposed electrode materials. It was believed that the introduction of CNFs may offer a conductive path to enhance the diffusion of ions, provide better structural support, and reduce the restacking of the MoS_2 layer during GCD cycles. Authors found that the MS/CNF-2 sample showed higher electrochemical behavior and an improved C_{sp} of 626.08 F/g at 1 A/g. In contrast, pristine MS showed a C_{sp} of 159.35 F/g, which is almost four times lower compared to the MS/CNF-2 sample. Tiwari et al. [133] stated that the hydrophilicity of the SC electrodes with minimal resistive losses are the most crucial parameters for the development of energy storage devices. In this connection, authors demonstrated the incorporation of MnO_2 and MoS_2 film-based heterostructures on CNTs. The MnO_2/CNT electrode showed a real capacitance and volumetric capacitance of 0.34 F/cm^2 and 6.5 F/cm^3, respectively. In a report by Chen et al. [134], the CNT@MoS_2 core–shell structure was obtained using the hydrothermal method. Authors found that MoS_2 has a hexagonal 2H-MoS_2 structure, which was confirmed by X-ray diffraction (XRD) and Raman spectroscopic measurements. The CNT@MoS_2 was used as an electrode modifier, and a C_{sp} of 87 F/g was obtained at 10 mV/s. Kumar et al. [135] prepared MoS_2-rGO (varying percentage of rGO; 5, 10, 15, and 20%) composites and explored them for energy storage applications. Authors obtained a C_{sp} of 1023 F/g at 1 A/g and a stability of 1000 cycles under optimized conditions. Farshadnia et al. [136] prepared a spongy nanostructured GO with a high surface area and decent porosity. The $CoNi_2S_4$ and MoS_2 were deposited on porous GO to improve the capacity and performance of the working electrode. The prepared $CoNi_2S_4$@MoS_2@rGO exhibited a C_{sp} of 3268 F/g at 1 A/g with 3000 stability cycles in a 3 M KOH electrolyte. Wei et al. [137] coated rGO onto NF and Ni_3S_2/MoS_2 composites under simple strategies at different times (18 h, 24 h, 30 h, 36 h, and 42 h). The time was optimized to investigate the effect of reaction time on the surface morphology of the electrode materials. It was observed that at 18 h and 24 h, Ni_3S_2/MoS_2 was formed with a 2D NS-like shape with a 3D network. The nanorods (NRs) obtained with increasing reaction time and hierarchical core–shell configuration were formed at 36 h at 150 °C. A C_{sp} of 6451 mF/cm^2 was obtained at 40 mA/cm^2 with a stability of 5000 cycles under optimized conditions for rGO/Ni_3S_2/MoS_2-based studies. Serrapede et al. [138] used 3D graphene aerogel-decorated MoS_2 as an electrode modifier

and achieved a decent C_{sp} of 210 F/g. In another report, Yan et al. [139] explored polymers as conductive supports to enhance the electrochemical performance of the MoS_2-based SCs. Authors prepared polypyrrole (PPy)-coated MoS_2 on CC and explored them for SC applications. The fabricated PPy/MoS_2/CC electrode showed a C_{sp} of 1150.4 mF/cm^2 at 5 mA/cm^2. Rajapriya et al. [140] used the hydrothermal method for the preparation of MoS_2/CNFs. Authors found that MoS_2/CNFs have a high surface area of 48 m^2/g, and the electrochemical investigation yielded a Csp of 903.9 F/g at 1 A/g with a cyclic stability of 5000 cycles. It was stated by the authors that nanoflowers of MoS_2 provided a void space between the NSs for the intercalation of electrolyte ions, which enhanced the performance of the MoS_2/CNFs. Arun et al. [141] proposed the hydrothermal preparation of Ni_3S_2/MoS_2/rGO hybrids on NF for SCs. The fabricated electrode with the Ni_3S_2/MoS_2/rGO hybrid on NF demonstrated a C_{sp} of 2580 F/g at 1 A/g and a stability of 10,000 cycles with 100% capacitance retention. Zhang et al. [142] reported the synthesis of a MoS_2-PPy@rGO composite using molybdenum oxide as the Mo source. The PPy was adopted as an intercalation agent to enlarge the interlayer space in MoS_2. The fabricated SCs exhibited an energy density of 134.4 μWh/cm^2 with a power density of 800 μW/cm^2. Rani et al. [143] adopted the hydrothermal approach for the fabrication of MoS_2/CNTs. The fabricated MoS_2/CNTs composite showed a C_{sp} of 436 F/g at 1 A/g. Liu et al. [144] reported the formation of N/O-co-doped carbon nanocages (NOCNs) modified with MoS_2 using the hydrothermal method. Authors found that ultrathin MoS_2 NSs were vertically grown on the NOCN surface, which can provide a fast pathway for electron transportation and prevent sheet aggregation. Authors observed that MoS_2@NOCN-3 demonstrated a C_{sp} of 240.8 F/g at 0.5 A/g. Aftab et al. [145] prepared a MoO_2/MoS_2@GO ternary hybrid composite by employing a wet chemical-aided method. The prepared MoO_2/MoS_2@GO ternary hybrid composite displayed decent electrochemical performance, and authors reported an acceptable C_{sp} of 1530 F/g at 2 A/g. Khandare et al. [146] reported a LiMoS_2/rGO-based electrode for energy storage applications, which demonstrated a power density of 686.3 W/kg and an energy density of 10.6 Wh/kg.

3.5. MoS_2 and Polymer Composite as Electrode Material

Li et al. [147] also used the in situ oxidative polymerization method for the preparation of a MoS_2/PPy composite. Authors obtained a Csp of 677.8 F/g at 1 A/g using an MP-2 electrode. Wang et al. [148] proposed the formation of a silicon dioxide (SiO_2) peristaltic supporting carbon (SPSC)/polyaniline (PANI)/MoS_2 composite for energy storage devices. Authors found that the proposed electrode displayed a C_{sp} of 637.5 F/g at 0.5 A/g with an energy density of 22.6 Wh/kg and a power density of 550 W/kg. A CuS/PANI@MoS_2 (CSPM) composite was prepared by Dai et al. [149]. This prepared CSPM composite showed a Csp value of 759.2 F/g at 1 A/g. Authors also reported a decent stability of 5000 cycles. Jasna et al. [150] have designed and fabricated a PANI/CNT/e-MoS_2 composite for SCs, which exhibited a C_{sp} of 532 F/g at 1 A/g. The proposed work also showed a stability of 4000 cycles with a high energy density of 11.8 Wh/kg. Suresh et al. [151] reported a C_{sp} of 177 F/g at a 0.5 current density using a cerium dioxide (CeO_2)/PANI/MoS_2 tri-composite as the electrode. Jhanjhariya et al. [152] fabricated a MoS_2/MWCNTs (MC) composite using the hydrothermal method, and PPy was incorporated using the in situ oxidation polymerization of a pyrrole monomer. The fabricated electrode (MCP1.5) exhibited a C_{sp} of 3352.08 F/g at 2 mV/s.

3.6. MoS_2 and MXene Composites as Electrode Material

In previous years, MXenes such as $Ti_3C_2T_x$ have attracted researchers because of their excellent electrochemical and conducting properties. Pan et al. [153] reported the

synthesis of a $Ti_3C_2T_x/MoS_2$ composite, which showed a Csp of 439 F/g at 5 mV/s with a stability of 10,000 cycles. Qiao et al. [154] designed and fabricated a flexible MXene/1T-MoS_2 composite paper electrode for SC applications, which exhibited specific area and volumetric capacitances of 561.2 mF/cm^2 and 1268.17 F/cm^3 at 0.8 mA/cm^2, respectively. Li et al. [155] reported that electrostatic spray deposition (ESD) is the most efficient method for the preparation of high-quality materials with improved electrochemical properties. Thus, authors used the ESD method for the preparation of a 1T $MoS_2/Ti_3C_2T_x$ composite, which showed C_{sp} of 1198 mF/cm^2 at 3 mA/cm^2 and cyclic stability for up to 7000 cycles. Ali et al. [156] designed and reported the synthesis of MoS_2@$Ti_3C_2T_x$ for SC applications. The fabricated electrode showed a Csp of 1022.7 F/g at 1 A/g with a cycle life of 5000 cycles. In another report by Bera et al. [157], a MoS_2 QDs/$Ti_3C_2T_x$-based electrode showed a decent Csp of 985 F/g and an energy density of 165.53 Wh/kg with a power density of 1100 W/kg. Hayat et al. [158] fabricated MoS_2@MXene//MXene flexible asymmetric SCs, which demonstrated a high energy density of 1.21 Wh/kg and a power density of 54.45 W/kg. The above reports show that MoS_2-based materials are promising candidates for SC applications. The electrochemical performance of the MoS_2-based electrode for SC applications is summarized in Table 2 [99–116,153,157,159,160].

Table 2. Electrochemical performance of MoS_2-based electrode for SC applications.

Electrode Modifier	Synthesis Method	Electrolyte	Stability Cycles	C_{sp} (F/g)	Current Density (A/g)	Refs.
MoS_2	Hydrothermal	3 M KOH	1000	205.41	0.25	[99]
1 T-MoS_2/CMS	Hydrothermal	1 M KOH	20,000	692	1	[100]
Polymer/MoS_2	Electro-deposition	PVA-H_2SO_4	-	130 mF/cm^3	5 mV/s	[101]
1T/2H-O-MoS_2@GF	Hydrothermal	1 M Na_2SO_4	10,000	280	1	[102]
2H-MoS_2	Hydrothermal	0.5 M H_2SO_4	5000	115.42	10 mV/s	[103]
MS-HT	Hydrothermal	6 M KOH	1200	742	5 mV/s	[104]
MS-MW	Hydrothermal	6 M KOH	1200	421	5 mV/s	[104]
MoS_2	Electro-deposition	1 M Na_2SO_4	-	416.9 mF/cm^2	1 mAcm^{-2}	[105]
Fc-1T-MoS_2	Electrochemical exfoliation	1 M H_2SO_4	2000	501	1	[106]
Few-layered 1T-MoS_2	Hydrothermal	Na_2SO_4	5000	250.3	1	[107]
Co-MoS_2	Hydrothermal	1 M KOH	10,000	86	1	[108]
N, Co doped MoS_2	Hydrothermal	6 M KOH	3000	1400	1	[109]
Ni-MoS_2/CC	Hydrothermal	0.5 M H_2SO_4	5000	305.9	1	[110]
Mn-MoS_2	Hydrothermal	0.5 M Na_2SO_4	5000	430	1	[111]
Fe-MoS_2	Hydrothermal	3 M KOH	2000	545	1	[112]
MoS_1Se_1	Hydrothermal	6 M KOH	6000	266.51	0.5	[113]
MnO_2/MoS_2	Ultrasonic/shearing	1 M Na_2SO_4	3000	224 mF cm^{-2}	-	[114]
MoS_2-RuO_2	Hydrothermal/Reduction	1 M KOH	10,000	972	1	[115]
SnO_2-MoS_2	Hydrothermal	3 M KOH	5000	415	1	[116]
$Ti_3C_2T_x/MoS_2$	Ultrasonic and heat treatment	3 M H_2SO_4	10,000	439	5 mV/s	[153]
S-rich MoS_2 QDs/MXene	Hydrothermal	1 M H_2SO_4	10,000	985	1	[157]
MoS_2–$Ti_3C_2T_x$	Hydrothermal	1 M H_2SO_4	10,000	303.8	1	[159]
Laser scribed graphene (LSG)/boron (B)-1 T MoS_2/MXene	Hydrothermal	PVA/K_2SO_4	10,000	72.31 mF/cm^2	0.075 mA/cm^2	[160]

4. Conclusions and Perspectives

Herein, we have reviewed MoS_2-based hybrid materials and concluded that they are promising for HER and SC applications. In the case of SCs, we have discussed the formation of various composites of MoS_2 with polymers, MXenes, metal oxides, CNTs, and rGO for the development of high-performance energy storage devices. It was observed that MoS_2-based materials with MXene show decent performance and stability. The observations

suggest that MoS_2-based materials have the potential for the construction of long-term stable SCs with decent performance. Various strategies have been employed to enhance the catalytic activity of MoS_2 for hydrogen production. One of the most effective approaches is modifying its electronic structure, which directly influences its physical properties and overall performance. On one hand, this modification increases the charge density, accelerates electron transport, and enhances conductivity. On the other hand, tuning the electronic structure optimizes hydrogen adsorption energy, a key factor in improving intrinsic catalytic activity. Moreover, the catalytic activity of hydrogen evolution reactions (HERs) can be further enhanced through several strategies. These include improving the intrinsic activity of catalytic sites by optimizing the electronic structure at the edges or activating the inert basal plane to enhance hydrogen adsorption, increasing the number of active sites by introducing defects such as cracks or holes in the MoS_2 layers, and boosting electrical conductivity by creating new electronic states near the Fermi level, thereby narrowing the bandgap. While significant progress has been made in designing and developing MoS_2-based electrocatalysts, there is still ample room for further advancements in the field. Current laboratory methods for synthesizing MoS_2 nanosheets typically yield only small quantities, limiting their feasibility for industrial applications. Therefore, developing scalable and efficient fabrication techniques is essential for enabling the mass production of MoS_2-based electrocatalysts. Literature reports indicate that the current method for evaluating the HER activity of MoS_2-based powder materials involves coating them onto glassy carbon electrodes (GCEs). This process requires binders like Nafion, which can hinder catalytic performance. A more effective approach to overcome this limitation is the direct growth of MoS_2 nanosheets on conductive substrates such as metal foils, fluorine-doped tin oxide (FTO), tin-doped indium oxide (ITO), carbon paper, or carbon cloth, ensuring better conductivity and stability. We believe that further advancements in this research field require enhancing the HER performance of MoS_2 by optimizing its electronic structure. This approach can effectively improve its physical properties, increase charge density, enhance conductivity, and facilitate electron transport.

Author Contributions: Conceptualization, K.A. and W.R.; writing—original draft preparation, K.A. and W.R.; writing—review and editing, T.H.O. and F.G.A.; supervision, T.H.O. and F.G.A. All authors have read and agreed to the published version of the manuscript.

Funding: This research received no external funding.

Conflicts of Interest: The authors declare no conflict of interest.

References

1. Raza, W.; Ahmad, K. Visible Light-Driven Photocatalysts for Environmental Applications Based on Graphitic Carbon Nitride. In *Handbook of Nanomaterials and Nanocomposites for Energy and Environmental Applications*; Springer International Publishing: Berlin/Heidelberg, Germany, 2020; pp. 1–25.
2. Raza, W.; Ahmad, K. Graphitic Carbon Nitride-Based Photocatalysts for Hydrogen Production. In *Sustainable Materials and Green Processing for Energy Conversion*; Elsevier: Amsterdam, The Netherlands, 2022; pp. 213–236, ISBN 9780128228388.
3. Raza, W.; Bahnemann, D.; Muneer, M. A Green Approach for Degradation of Organic Pollutants Using Rare Earth Metal Doped Bismuth Oxide. *Catal. Today* **2018**, *300*, 89–98. [CrossRef]
4. Raza, W.; Ahmad, K.; Kim, H. Fabrication of Defective Graphene Oxide for Efficient Hydrogen Production and Enhanced 4-Nitro-Phenol Reduction. *Nanotechnology* **2021**, *32*, 495404. [CrossRef] [PubMed]
5. Raza, W.; Tesler, A.B.; Anca, M.; Schmuki, P. Solar Light-Induced Photoelectrochemical H_2 Generation Over Hierarchical TiO_2 Nanotube Arrays Decorated with CdS Nanoparticles. *J. Electrochem. Soc.* **2024**, *171*, 066506. [CrossRef]
6. Raza, W.; Tesler, A.B.; Mazare, A.; Tomanec, O.; Kment, S.; Schmuki, P. Pt Single Atoms as Co-Catalysts on CdS-Sensitized Single-Crystalline TiO_2 Nanoflakes for Enhanced Visible Light Photocatalytic H_2 Generation. *ChemCatChem* **2023**, *15*, e202300327. [CrossRef]

7. Raza, W.; Ahmad, K. Recent Progress on Perovskite-Based Solar Cells. In *Perovskite Materials for Energy and Environmental Applications*; John Wiley & Sons, Ltd.: Hoboken, NJ, USA, 2021; pp. 147–165, ISBN 9781119763376.
8. Osuagwu, B.; Raza, W.; Tesler, A.B.; Schmuki, P. A Drastic Improvement in Photocatalytic H_2 production by TiO_2 nanosheets Grown Directly on Ta_2O_5 substrates. *Nanoscale* **2021**, *13*, 12750–12756. [CrossRef]
9. Zhang, Y.; Wang, L.; Chen, Q.; Cao, J.; Zhang, C. Recent Progress of Electrochemical Hydrogen Evolution over 1T-MoS_2 Catalysts. *Front. Chem.* **2022**, *10*, 1000406. [CrossRef]
10. Zhang, L.; Shi, Z.; Lin, Y.; Chong, F.; Qi, Y. Design Strategies for Large Current Density Hydrogen Evolution Reaction. *Front. Chem.* **2022**, *10*, 866415. [CrossRef]
11. Gong, F.; Liu, M.; Gong, L.; Ye, S.; Jiang, Q.; Zeng, G.; Zhang, X.; Peng, Z.; Zhang, Y.; Fang, S.; et al. Modulation of Mo–Fe–C Sites Over Mesoscale Diffusion-Enhanced Hollow Sub-Micro Reactors Toward Boosted Electrochemical Water Oxidation. *Adv. Funct. Mater.* **2022**, *32*, 2202141. [CrossRef]
12. Ma, Y.; Leng, D.; Zhang, X.; Fu, J.; Pi, C.; Zheng, Y.; Gao, B.; Li, X.; Li, N.; Chu, P.K.; et al. Enhanced Activities in Alkaline Hydrogen and Oxygen Evolution Reactions on MoS_2 Electrocatalysts by In-Plane Sulfur Defects Coupled with Transition Metal Doping. *Small* **2022**, *18*, 2203173. [CrossRef]
13. Wang, G.; Zhang, G.; Ke, X.; Chen, X.; Chen, X.; Wang, Y.; Huang, G.; Dong, J.; Chu, S.; Sui, M. Direct Synthesis of Stable 1T-MoS_2 Doped with Ni Single Atoms for Water Splitting in Alkaline Media. *Small* **2022**, *18*, 2107238. [CrossRef] [PubMed]
14. Li, J.; Tang, C.; Zhang, H.; Zou, Z.; Li, C.M. Mesoporous molybdenum carbide for greatly enhanced hydrogen evolution at high current density and its mechanism studies. *Mater. Rep. Energy* **2023**, *3*, 100215. [CrossRef]
15. Abdelghafar, F.; Xu, X.; Jiang, S.P.; Shao, Z. Designing single-atom catalysts toward improved alkaline hydrogen evolution reaction. *Mater. Rep. Energy* **2022**, *2*, 100144. [CrossRef]
16. Hu, C.; Zhang, L.; Gong, J. Recent Progress Made in the Mechanism Comprehension and Design of Electrocatalysts for Alkaline Water Splitting. *Energy Environ. Sci.* **2019**, *12*, 2620–2645. [CrossRef]
17. Zhang, Z.; Cong, L.; Yu, Z.; Qu, L.; Huang, W. Facial Synthesis of Fe–Ni Bimetallic N-Doped Carbon Framework for Efficient Electrochemical Hydrogen Evolution Reaction. *Mater. Today Energy* **2020**, *16*, 100387. [CrossRef]
18. Faber, M.S.; Jin, S. Earth-Abundant Inorganic Electrocatalysts and Their Nanostructures for Energy Conversion Applications. *Energy Environ. Sci.* **2014**, *7*, 3519–3542. [CrossRef]
19. Anjum, M.A.R.; Lee, M.H.; Lee, J.S. BCN Network-Encapsulated Multiple Phases of Molybdenum Carbide for Efficient Hydrogen Evolution Reactions in Acidic and Alkaline Media. *J. Mater. Chem. A* **2017**, *5*, 13122–13129. [CrossRef]
20. Anjum, M.A.R.; Lee, J.S. Sulfur and Nitrogen Dual-Doped Molybdenum Phosphide Nanocrystallites as an Active and Stable Hydrogen Evolution Reaction Electrocatalyst in Acidic and Alkaline Media. *ACS Catal.* **2017**, *7*, 3030–3038. [CrossRef]
21. Zou, X.; Zhang, Y. Noble Metal-Free Hydrogen Evolution Catalysts for Water Splitting. *Chem. Soc. Rev.* **2015**, *44*, 5148–5180. [CrossRef]
22. Jiang, Y.; Lu, Y. Designing Transition-Metal-Boride-Based Electrocatalysts for Applications in Electrochemical Water Splitting. *Nanoscale* **2020**, *12*, 9327–9351. [CrossRef]
23. Boyjoo, Y.; Shi, H.; Tian, Q.; Liu, S.; Liang, J.; Wu, Z.S.; Jaroniec, M.; Liu, J. Engineering Nanoreactors for Metal-Chalcogen Batteries. *Energy Environ. Sci.* **2021**, *14*, 540–575. [CrossRef]
24. Peng, O.; Shi, R.; Wang, J.; Zhang, X.; Miao, J.; Zhang, L.; Fu, Y.; Madhusudan, P.; Liu, K.; Amini, A.; et al. Hierarchical Heterostructured Nickle Foam–Supported Co_3S_4 Nanorod Arrays Embellished with Edge-Exposed MoS_2 Nanoflakes for Enhanced Alkaline Hydrogen Evolution Reaction. *Mater. Today Energy* **2020**, *18*, 100513. [CrossRef]
25. Thomas, N.; Mathew, S.; Nair, K.M.; O'Dowd, K.; Forouzandeh, P.; Goswami, A.; McGranaghan, G.; Pillai, S.C. 2D MoS_2: Structure, Mechanisms, and Photocatalytic Applications. *Mater. Today Sustain.* **2021**, *13*, 100073. [CrossRef]
26. Chen, J.; Liu, G.; Zhu, Y.Z.; Su, M.; Yin, P.; Wu, X.J.; Lu, Q.; Tan, C.; Zhao, M.; Liu, Z.; et al. Ag@MoS_2 Core-Shell Heterostructure as SERS Platform to Reveal the Hydrogen Evolution Active Sites of Single-Layer MoS_2. *J. Am. Chem. Soc.* **2020**, *142*, 7161–7167. [CrossRef]
27. Gong, F.; Ye, S.; Liu, M.; Zhang, J.; Gong, L.; Zeng, G.; Meng, E.; Su, P.; Xie, K.; Zhang, Y.; et al. Boosting Electrochemical Oxygen Evolution over Yolk-Shell Structured O–MoS_2 Nanoreactors with Sulfur Vacancy and Decorated Pt Nanoparticles. *Nano Energy* **2020**, *78*, 105284. [CrossRef]
28. Zhang, C.; Zhang, Y.; Zhang, Y.; Huang, X.; Li, Y.; Cao, J.; Zhou, C. One-Pot Synthesis of Ultrathin 1T-MoS_2 Nanosheets as Efficient Catalyst for Reduction of 4-Nitrophenol. *Mater. Lett.* **2022**, *314*, 131794. [CrossRef]
29. Meng, C.; Chen, X.; Gao, Y.; Zhao, Q.; Kong, D.; Lin, M.; Chen, X.; Li, Y.; Zhou, Y. Recent Modification Strategies of MoS_2 for Enhanced Electrocatalytic Hydrogen Evolution. *Molecules* **2020**, *25*, 1136. [CrossRef]
30. Lu, F.; Zhou, M.; Zhou, Y.; Zeng, X. First-Row Transition Metal Based Catalysts for the Oxygen Evolution Reaction under Alkaline Conditions: Basic Principles and Recent Advances. *Small* **2017**, *13*, 1701931. [CrossRef]
31. Zhu, C.; Gao, D.; Ding, J.; Chao, D.; Wang, J. TMD-Based Highly Efficient Electrocatalysts Developed by Combined Computational and Experimental Approaches. *Chem. Soc. Rev.* **2018**, *47*, 4332–4356. [CrossRef]

32. Tang, Q.; Jiang, D.E. Stabilization and Band-Gap Tuning of the 1T-MoS_2 Monolayer by Covalent Functionalization. *Chem. Mater.* **2015**, *27*, 3743–3748. [CrossRef]
33. Jin, Q.; Liu, N.; Chen, B.; Mei, D. Mechanisms of Semiconducting 2H to Metallic 1T Phase Transition in Two-Dimensional MoS_2 Nanosheets. *J. Phys. Chem. C* **2018**, *122*, 28215–28224. [CrossRef]
34. Benson, E.E.; Zhang, H.; Schuman, S.A.; Nanayakkara, S.U.; Bronstein, N.D.; Ferrere, S.; Blackburn, J.L.; Miller, E.M. Balancing the Hydrogen Evolution Reaction, Surface Energetics, and Stability of Metallic MoS_2 Nanosheets via Covalent Functionalization. *J. Am. Chem. Soc.* **2018**, *140*, 441–450. [CrossRef]
35. Liu, L.; Liu, N.; Chen, B.; Dai, C.; Wang, N. Recent Modification Strategies of MoS_2 towards Electrocatalytic Hydrogen Evolution. *Catalysts* **2024**, *14*, 126. [CrossRef]
36. Tributsch, H.; Bennett, J.C. Electrochemistry and Photochemistry of MoS_2 Layer Crystals. I. *J. Electroanal. Chem.* **1977**, *81*, 97–111. [CrossRef]
37. Hinnemann, B.; Moses, P.G.; Bonde, J.; Jørgensen, K.P.; Nielsen, J.H.; Horch, S.; Chorkendorff, I.; Nørskov, J.K. Biomimetic Hydrogen Evolution: MoS_2 Nanoparticles as Catalyst for Hydrogen Evolution. *J. Am. Chem. Soc.* **2005**, *127*, 5308–5309. [CrossRef]
38. Anjum, M.A.R.; Jeong, H.Y.; Lee, M.H.; Shin, H.S.; Lee, J.S. Efficient Hydrogen Evolution Reaction Catalysis in Alkaline Media by All-in-One MoS_2 with Multifunctional Active Sites. *Adv. Mater.* **2018**, *30*, 1707105. [CrossRef]
39. Jaramillo, T.F.; Jørgensen, K.P.; Bonde, J.; Nielsen, J.H.; Horch, S.; Chorkendorff, I. Identification of Active Edge Sites for Electrochemical H_2 Evolution from MoS_2 Nanocatalysts. *Science* **2007**, *317*, 100–102. [CrossRef]
40. Dang, V.D.; Putikam, R.; Lin, M.-C.; Wei, K.-H. MoS_2 Nanoflowers Grown on Plasma-Induced W-Anchored Graphene for Efficient and Stable H_2 Production Through Seawater Electrolysis. *Small* **2024**, *20*, 2305220. [CrossRef]
41. Dang, V.D.; Hsiao, C.-Y.; Le, P.A.; Le, V.Q.; Thao, D.H.P.; Do, T.-H.; Wei, K.-H. Surface-Plasma-Induced One-Pot Synthesis of N,S-Carbon Dot Intercalated MoS_2/Graphene Nanosheets for Highly Efficient Hydrogen Evolution Reaction. *ACS Appl. Energy Mater.* **2022**, *5*, 12817–12827. [CrossRef]
42. Nguyen, V.-T.; Le, P.A.; Hsu, Y.-C.; Wei, K.-H. Plasma-Induced Exfoliation Provides Onion-Like Graphene-Surrounded MoS_2 Nanosheets for a Highly Efficient Hydrogen Evolution Reaction. *ACS Appl. Mater. Interfaces* **2020**, *12*, 11533–11542. [CrossRef]
43. Nguyen, V.-T.; Yang, T.-Y.; Le, P.A.; Yen, P.-J.; Chueh, Y.-L.; Wei, K.-H. New Simultaneous Exfoliation and Doping Process for Generating MX_2 Nanosheets for Electrocatalytic Hydrogen Evolution Reaction. *ACS Appl. Mater. Interfaces* **2019**, *11*, 14786–14795. [CrossRef]
44. Vesborg, P.C.K.; Seger, B.; Chorkendorff, I. Recent Development in Hydrogen Evolution Reaction Catalysts and Their Practical Implementation. *J. Phys. Chem. Lett.* **2015**, *6*, 951–957. [CrossRef]
45. Huang, Z.; Chen, Z.; Chen, Z.; Lv, C.; Humphrey, M.G.; Zhang, C. Cobalt Phosphide Nanorods as an Efficient Electrocatalyst for the Hydrogen Evolution Reaction. *Nano Energy* **2014**, *9*, 373–382. [CrossRef]
46. Yu, P.; Wang, F.; Shifa, T.A.; Zhan, X.; Lou, X.; Xia, F.; He, J. Earth Abundant Materials beyond Transition Metal Dichalcogenides: A Focus on Electrocatalyzing Hydrogen Evolution Reaction. *Nano Energy* **2019**, *58*, 244–276. [CrossRef]
47. Mahmood, N.; Yao, Y.; Zhang, J.W.; Pan, L.; Zhang, X.; Zou, J.J. Electrocatalysts for Hydrogen Evolution in Alkaline Electrolytes: Mechanisms, Challenges, and Prospective Solutions. *Adv. Sci.* **2018**, *5*, 1700464. [CrossRef]
48. Wang, J.; Zhang, H.; Wang, X. Recent Methods for the Synthesis of Noble-Metal-Free Hydrogen-Evolution Electrocatalysts: From Nanoscale to Sub-Nanoscale. *Small Methods* **2017**, *1*, 1700118. [CrossRef]
49. Duan, X.; Xu, J.; Wei, Z.; Ma, J.; Guo, S.; Liu, H.; Dou, S. Atomically Thin Transition-Metal Dichalcogenides for Electrocatalysis and Energy Storage. *Small Methods* **2017**, *1*, 1700156. [CrossRef]
50. Morales-Guio, C.G.; Stern, L.A.; Hu, X. Nanostructured Hydrotreating Catalysts for Electrochemical Hydrogen Evolution. *Chem. Soc. Rev.* **2014**, *43*, 6555–6569. [CrossRef] [PubMed]
51. Sun, Y.; Gao, S.; Lei, F.; Xiao, C.; Xie, Y. Ultrathin Two-Dimensional Inorganic Materials: New Opportunities for Solid State Nanochemistry. *Acc. Chem. Res.* **2015**, *48*, 3–12. [CrossRef] [PubMed]
52. Novoselov, K.S.; Jiang, D.; Schedin, F.; Booth, T.J.; Khotkevich, V.V.; Morozov, S.V.; Geim, A.K. Two-Dimensional Atomic Crystals. *Proc. Natl. Acad. Sci. USA* **2005**, *102*, 10451–10453. [CrossRef]
53. Li, T.; Galli, G. Electronic Properties of MoS_2 Nanoparticles. *J. Phys. Chem. C* **2007**, *111*, 16192–16196. [CrossRef]
54. Lukowski, M.A.; Daniel, A.S.; Meng, F.; Forticaux, A.; Li, L.; Jin, S. Enhanced Hydrogen Evolution Catalysis from Chemically Exfoliated Metallic MoS_2 Nanosheets. *J. Am. Chem. Soc.* **2013**, *135*, 10274–10277. [CrossRef]
55. Liu, P.; Zhu, J.; Zhang, J.; Xi, P.; Tao, K.; Gao, D.; Xue, D. P Dopants Triggered New Basal Plane Active Sites and Enlarged Interlayer Spacing in MoS_2 Nanosheets toward Electrocatalytic Hydrogen Evolution. *ACS Energy Lett.* **2017**, *2*, 745–752. [CrossRef]
56. Jin, Q.; Liu, N.; Dai, C.; Xu, R.; Wu, B.; Yu, G.; Chen, B.; Du, Y. H2-Directing Strategy on In Situ Synthesis of Co-MoS_2 with Highly Expanded Interlayer for Elegant HER Activity and Its Mechanism. *Adv. Energy Mater.* **2020**, *10*, 2000291. [CrossRef]
57. Zhang, H.; Xu, H.; Wang, L.; Ouyang, C.; Liang, H.; Zhong, S. A Metal–Organic Frameworks Derived 1T-MoS_2 with Expanded Layer Spacing for Enhanced Electrocatalytic Hydrogen Evolution. *Small* **2023**, *19*, 2205736. [CrossRef] [PubMed]

58. Hu, W.; Liu, H.; Dong, W.; Akif Munir, H.; Fan, X.; Tian, X.; Pang, L. Ammonium Ions Intercalated 1T/2H-MoS_2 with Increased Interlayer Spacing for High-Efficient Electrocatalytic Hydrogen Evolution Reaction. *J. Electroanal. Chem.* **2023**, *949*, 117882. [CrossRef]
59. Xie, J.; Yang, X.; Xie, Y. Defect Engineering in Two-Dimensional Electrocatalysts for Hydrogen Evolution. *Nanoscale* **2020**, *12*, 4283–4294. [CrossRef] [PubMed]
60. Du, X.; Huang, J.; Zhang, J.; Yan, Y.; Wu, C.; Hu, Y.; Yan, C.; Lei, T.; Chen, W.; Fan, C.; et al. Modulating Electronic Structures of Inorganic Nanomaterials for Efficient Electrocatalytic Water Splitting. *Angew. Chemie-Int. Ed.* **2019**, *58*, 4484–4502. [CrossRef] [PubMed]
61. Zhang, H.; Yu, L.; Chen, T.; Zhou, W.; Lou, X.W. (David) Surface Modulation of Hierarchical MoS_2 Nanosheets by Ni Single Atoms for Enhanced Electrocatalytic Hydrogen Evolution. *Adv. Funct. Mater.* **2018**, *28*, 1807086. [CrossRef]
62. Luo, Z.; Ouyang, Y.; Zhang, H.; Xiao, M.; Ge, J.; Jiang, Z.; Wang, J.; Tang, D.; Cao, X.; Liu, C.; et al. Chemically Activating MoS_2 via Spontaneous Atomic Palladium Interfacial Doping towards Efficient Hydrogen Evolution. *Nat. Commun.* **2018**, *9*, 2120. [CrossRef]
63. Sun, X.; Dai, J.; Guo, Y.; Wu, C.; Hu, F.; Zhao, J.; Zeng, X.; Xie, Y. Semimetallic Molybdenum Disulfide Ultrathin Nanosheets as an Efficient Electrocatalyst for Hydrogen Evolution. *Nanoscale* **2014**, *6*, 8359–8367. [CrossRef]
64. Xiong, Q.; Wang, Y.; Liu, P.F.; Zheng, L.R.; Wang, G.; Yang, H.G.; Wong, P.K.; Zhang, H.; Zhao, H. Cobalt Covalent Doping in MoS_2 to Induce Bifunctionality of Overall Water Splitting. *Adv. Mater.* **2018**, *30*, 1801450. [CrossRef] [PubMed]
65. Wang, J.; Fang, W.; Hu, Y.; Zhang, Y.; Dang, J.; Wu, Y.; Chen, B.; Zhao, H.; Li, Z. Single Atom Ru Doping 2H-MoS_2 as Highly Efficient Hydrogen Evolution Reaction Electrocatalyst in a Wide PH Range. *Appl. Catal. B Environ.* **2021**, *298*, 120490. [CrossRef]
66. Sun, H.; Yan, Z.; Liu, F.; Xu, W.; Cheng, F.; Chen, J. Self-Supported Transition-Metal-Based Electrocatalysts for Hydrogen and Oxygen Evolution. *Adv. Mater.* **2020**, *32*, 1806326. [CrossRef]
67. Fu, Q.; Han, J.; Wang, X.; Xu, P.; Yao, T.; Zhong, J.; Zhong, W.; Liu, S.; Gao, T.; Zhang, Z.; et al. 2D Transition Metal Dichalcogenides: Design, Modulation, and Challenges in Electrocatalysis. *Adv. Mater.* **2021**, *33*, 1907818. [CrossRef]
68. Li, Z.; Hu, M.; Wang, P.; Liu, J.; Yao, J.; Li, C. Heterojunction Catalyst in Electrocatalytic Water Splitting. *Coord. Chem. Rev.* **2021**, *439*, 213953. [CrossRef]
69. Hao, J.; Hu, H.; Dong, Y.; Hu, J.; Sang, X.; Duan, F.; Lu, S.; Zhu, H.; Du, M. Interface Engineering in Core-Shell Co9S8@MoS_2nanocrystals Induces Enhanced Hydrogen Evolution in Acidic and Alkaline Media. *New J. Chem.* **2021**, *45*, 11167–11173. [CrossRef]
70. Liu, Q.; Fang, Q.; Chu, W.; Wan, Y.; Li, X.; Xu, W.; Habib, M.; Tao, S.; Zhou, Y.; Liu, D.; et al. Electron-Doped 1T-MoS_2 via Interface Engineering for Enhanced Electrocatalytic Hydrogen Evolution. *Chem. Mater.* **2017**, *29*, 4738–4744. [CrossRef]
71. Li, H.; Yu, K.; Li, C.; Tang, Z.; Guo, B.; Lei, X.; Fu, H.; Zhu, Z. Charge-Transfer Induced High Efficient Hydrogen Evolution of MoS_2/Graphene Cocatalyst. *Sci. Rep.* **2015**, *5*, 18730. [CrossRef]
72. Gong, F.; Liu, M.; Ye, S.; Gong, L.; Zeng, G.; Xu, L.; Zhang, X.; Zhang, Y.; Zhou, L.; Fang, S.; et al. All-PH Stable Sandwich-Structured MoO_2/MoS_2/C Hollow Nanoreactors for Enhanced Electrochemical Hydrogen Evolution. *Adv. Funct. Mater.* **2021**, *31*, 2101715. [CrossRef]
73. Fu, W.; He, H.; Zhang, Z.; Wu, C.; Wang, X.; Wang, H.; Zeng, Q.; Sun, L.; Wang, X.; Zhou, J.; et al. Strong Interfacial Coupling of MoS2/g-C3N4 van de Waals Solids for Highly Active Water Reduction. *Nano Energy* **2016**, *27*, 44–50. [CrossRef]
74. Chen, W.; Gu, J.; Du, Y.; Song, F.; Bu, F.; Li, J.; Yuan, Y.; Luo, R.; Liu, Q.; Zhang, D. Achieving Rich and Active Alkaline Hydrogen Evolution Heterostructures via Interface Engineering on 2D 1T-MoS_2 Quantum Sheets. *Adv. Funct. Mater.* **2020**, *30*, 2000551. [CrossRef]
75. Hu, J.; Zhang, C.; Zhang, Y.; Yang, B.; Qi, Q.; Sun, M.; Zi, F.; Leung, M.K.H.; Huang, B. Interface Modulation of MoS_2/Metal Oxide Heterostructures for Efficient Hydrogen Evolution Electrocatalysis. *Small* **2020**, *16*, 2002212. [CrossRef] [PubMed]
76. Wu, J.; Wang, X.; Jiang, J.; Lin, W.; Zhu, S.; Sha, J.; Ma, L.; Zhao, N. In-Situ Synthesis of MoS_2/Co_9S_8 Heterostructure for Efficient HER Electrocatalyst. *Mater. Lett.* **2021**, *292*, 129621. [CrossRef]
77. Luo, M.; Liu, S.; Zhu, W.; Ye, G.; Wang, J.; He, Z. An Electrodeposited MoS_2-MoO_{3-x}/Ni_3S_2 Heterostructure Electrocatalyst for Efficient Alkaline Hydrogen Evolution. *Chem. Eng. J.* **2022**, *428*, 131055. [CrossRef]
78. Meng, X.; Yu, L.; Ma, C.; Nan, B.; Si, R.; Tu, Y.; Deng, J.; Deng, D.; Bao, X. Three-Dimensionally Hierarchical MoS_2/Graphene Architecture for High-Performance Hydrogen Evolution Reaction. *Nano Energy* **2019**, *61*, 611–616. [CrossRef]
79. Yilmaz, G.; Yang, T.; Du, Y.; Yu, X.; Feng, Y.P.; Shen, L.; Ho, G.W. Stimulated Electrocatalytic Hydrogen Evolution Activity of MOF-Derived MoS_2 Basal Domains via Charge Injection through Surface Functionalization and Heteroatom Doping. *Adv. Sci.* **2019**, *6*, 1900140. [CrossRef]
80. Kim, M.; Anjum, M.A.R.; Lee, M.; Lee, B.J.; Lee, J.S. Activating MoS_2 Basal Plane with Ni_2P Nanoparticles for Pt-Like Hydrogen Evolution Reaction in Acidic Media. *Adv. Funct. Mater.* **2019**, *29*, 1809151. [CrossRef]
81. Hu, J.; Zhang, C.; Yang, P.; Xiao, J.; Deng, T.; Liu, Z.; Huang, B.; Leung, M.K.H.; Yang, S. Kinetic-Oriented Construction of MoS_2 Synergistic Interface to Boost PH-Universal Hydrogen Evolution. *Adv. Funct. Mater.* **2020**, *30*, 1908520. [CrossRef]

82. Zhou, F.; Zhang, X.; Sa, R.; Zhang, S.; Wen, Z.; Wang, R. The Electrochemical Overall Water Splitting Promoted by MoS_2 in Coupled Nickel–Iron (Oxy)Hydride/Molybdenum Sulfide/Graphene Composite. *Chem. Eng. J.* **2020**, *397*, 125454. [CrossRef]
83. Kim, M.; Anjum, M.A.R.; Choi, M.; Jeong, H.Y.; Choi, S.H.; Park, N.; Lee, J.S. Covalent 0D–2D Heterostructuring of Co_9S_8–MoS_2 for Enhanced Hydrogen Evolution in All PH Electrolytes. *Adv. Funct. Mater.* **2020**, *30*, 2002536. [CrossRef]
84. Wei, Y.; Lv, Y.; Guo, B.; Gong, J. Hierarchical Molybdenum Disulfide Nanosheet Arrays Stemmed from Nickel-Cobalt Layered Double Hydroxide/Carbon Cloth for Highly-Efficient Hydrogen Evolution Reaction. *J. Energy Chem.* **2021**, *57*, 587–592. [CrossRef]
85. Lu, Z.; Liang, D.; Ping, X.; Xing, L.; Wang, Z.; Wu, L.; Lu, P.; Jiao, L. 1D/2D Heterostructures as Ultrathin Catalysts for Hydrogen Evolution Reaction. *Small* **2020**, *16*, 2004296. [CrossRef] [PubMed]
86. Liu, Q.; Xue, Z.; Jia, B.; Liu, Q.; Liu, K.; Lin, Y.; Liu, M.; Li, Y.; Li, G. Hierarchical Nanorods of MoS_2/MoP Heterojunction for Efficient Electrocatalytic Hydrogen Evolution Reaction. *Small* **2020**, *16*, 2002482. [CrossRef]
87. Tu, Y.; Deng, J.; Ma, C.; Yu, L.; Bao, X.; Deng, D. Double-Layer Hybrid Chainmail Catalyst for High-Performance Hydrogen Evolution. *Nano Energy* **2020**, *72*, 104700. [CrossRef]
88. Huang, X.; Xu, H.; Cao, D.; Cheng, D. Interface Construction of P-Substituted MoS_2 as Efficient and Robust Electrocatalyst for Alkaline Hydrogen Evolution Reaction. *Nano Energy* **2020**, *78*, 105253. [CrossRef]
89. Kim, M.; Seok, H.; Clament Sagaya Selvam, N.; Cho, J.; Choi, G.H.; Nam, M.G.; Kang, S.; Kim, T.; Yoo, P.J. Kirkendall Effect Induced Bifunctional Hybrid Electrocatalyst (Co_9S_8@MoS_2/N-Doped Hollow Carbon) for High Performance Overall Water Splitting. *J. Power Sources* **2021**, *493*, 229688. [CrossRef]
90. Sun, Q.; Tong, Y.; Chen, P.; Zhou, B.; Dong, X. Universal Strategy of Bimetal Heterostructures as Superior Bifunctional Catalysts for Electrochemical Water Splitting. *ACS Sustain. Chem. Eng.* **2021**, *9*, 4206–4212. [CrossRef]
91. Zhang, C.L.; Xie, Y.; Liu, J.T.; Cao, F.H.; Cong, H.P.; Li, H. 1D Core−Shell MOFs Derived CoP Nanoparticles-Embedded N-Doped Porous Carbon Nanotubes Anchored with MoS_2 Nanosheets as Efficient Bifunctional Electrocatalysts. *Chem. Eng. J.* **2021**, *419*, 129977. [CrossRef]
92. Li, X.; Lv, X.; Sun, X.; Yang, C.; Zheng, Y.-Z.; Yang, L.; Li, S.; Tao, X. Edge-oriented, high-percentage 1T′-phase MoS_2 nanosheets stabilize Ti_3C_2 MXene for efficient electrocatalytic hydrogen evolution. *Appl. Catal. B Environ.* **2021**, *284*, 119708. [CrossRef]
93. Chen, L.; Liang, J.; Zhang, Q.; Hu, X.; Peng, W.; Li, Y.; Zhang, F.; Fan, X. Quasi zero-dimensional MoS_2 quantum dots decorated 2D Ti3C2Tx MXene as advanced electrocatalysts for hydrogen evolution reaction. *Int. J. Hydrogen Energy* **2022**, *47*, 10583–10593. [CrossRef]
94. Chen, Y.; Meng, G.; Yang, T.; Chen, C.; Chang, Z.; Kong, F.; Tian, H.; Cui, X.; Hou, X.; Shi, J. Interfacial engineering of Co-doped 1T-MoS_2 coupled with V2C MXene for efficient electrocatalytic hydrogen evolution. *Chem. Eng. J.* **2022**, *450*, 138157. [CrossRef]
95. Ma, S.; Xu, Z.; Jia, Z.; Chen, L.; Zhu, H.; Chen, Y.; Guo, X.; Du, M. Facile fabrication of carbon fiber skeleton structure of MoS_2 supported on 2D MXene composite with highly efficient and stable hydrogen evolution reaction. *Compos. Sci. Technol.* **2022**, *222*, 109380. [CrossRef]
96. Tang, C.-K.; Zheng, X.; Chen, X.-L.; Fu, Y.-G.; Lü, Q.-F. Defect-rich MoS_2/CoS_2 on $Mo_2TiC_2T_x$ MXene as an efficient catalyst for hydrogen evolution reaction in acidic media. *FlatChem* **2023**, *42*, 100581. [CrossRef]
97. Raj, S.K.; Sharma, V.; Mishra, S.; Kulshrestha, V. MoS_2 quantum dot-modified MXene nanoflowers for efficient electrocatalytic hydrogen evolution reaction. *RSC Appl. Interfaces* **2024**, *1*, 1057–1068. [CrossRef]
98. Samawi, K.A.; Abdulrazzaq, S.J.; Zorah, M.; Al-Bahrani, M.; Mahmoud, H.M.A.; Abdulkareem-Alsultan, G.; Taki, A.G.; Nassar, M.F. MoS_2/graphdiyne nanotube/MXene 3D-interconnected ternary aerogel: A high-performance electrocatalyst for hydrogen evolution reaction. *J. Solid State Chem.* **2024**, *334*, 124690. [CrossRef]
99. Gupta, H.; Chakrabarti, S.; Mothkuri, S.; Padya, B.; Rao, T.N.; Jain, P.K. High performance supercapacitor based on 2D-MoS_2 nanostructures. *Mater. Today Proc.* **2020**, *26*, 20–24. [CrossRef]
100. Joseph, N.; Bose, A.C. Construction of few layered metallic MoS_2 microspheres using glucose induced carbon spheres and its application in symmetric supercapacitor device. *J. Electroanal. Chem.* **2020**, *874*, 114461. [CrossRef]
101. Varasteanu, P.; Romanitan, C.; Bratosin, I.; Djourelov, N.; Gavrila, R.; Radoi, A.; Kusko, M. Exploring the impact of MoS_2 on the performance of the planar solid micro-supercapacitor. *Mater. Chem. Phys.* **2021**, *265*, 124490. [CrossRef]
102. Lee, S.; Hwang, J.; Kim, D.; Ahn, H. Oxygen incorporated in 1T/2H hybrid MoS_2 nanoflowers prepared from molybdenum blue solution for asymmetric supercapacitor applications. *Chem. Eng. J.* **2021**, *419*, 129701. [CrossRef]
103. Shrivastav, M.; Kushwaha, H.S.; Dhiman, R. 2H-MoS_2 as an electrode material for oxygen reduction reaction and supercapacitor applications. *Mater. Today Proc.* 2022, *in press*. [CrossRef]
104. Kour, P.; Deeksha; Yadav, K. Electrochemical performance of mixed-phase 1T/2H MoS_2 synthesized by conventional hydrothermal v/s microwave-assisted hydrothermal method for supercapacitor applications. *J. Alloys Compd.* **2022**, *922*, 166194. [CrossRef]
105. Teli, A.M.; Beknalkar, S.A.; Mane, S.M.; Bhat, T.S.; Kamble, B.B.; Patil, S.B.; Sadale, S.B.; Shin, J.C. Electrodeposited crumpled MoS_2 nanoflakes for asymmetric supercapacitor. *Ceram. Int.* **2022**, *48*, 29002–29010. [CrossRef]
106. Naz, R.; Abbas, W.; Liu, Q.; Shafi, S.; Gull, S.; Khan, S.; Rasheed, T.; Song, G.; Gu, J. Covalent functionalization of electrochemically exfoliated 1T-MoS_2 nanosheets for high-performance supercapacitor electrode. *J. Alloys Compd.* **2023**, *951*, 169944. [CrossRef]

107. Xu, J.; Yuan, X.; Zhao, Y.; Rui, S.; Jia, Q.; Li, H.; Lu, S.; Li, B.; Zhang, Y.; Zhu, X. One-step hydrothermal synthesis of few-layered metallic phase MoS_2 for high-performance supercapacitors. *Prog. Nat. Sci. Mater. Int.* **2024**, *34*, 429–436. [CrossRef]
108. Rohith, R.; Manuraj, M.; Jafri, R.I.; Rakhi, R.B. Co-MoS_2 nanoflower coated carbon fabric as a flexible electrode for supercapacitor. *Mater. Today Proc.* **2022**, *50*, 1–6. [CrossRef]
109. Fayed, M.G.; Attia, S.Y.; Barakat, Y.F.; El-Shereafy, E.E.; Rashad, M.M.; Mohamed, S.G. Carbon and nitrogen co-doped MoS_2 nanoflakes as an electrode material for lithium-ion batteries and supercapacitors. *Sustain. Mater. Technol.* **2021**, *29*, e00306. [CrossRef]
110. Saseendran, S.B.; Ashok, A.; Asha, A.S. Flexible and binder-free supercapacitor electrode with high mass loading using transition metal doped MoS_2 nanostructures. *J. Alloys Compd.* **2023**, *968*, 172131. [CrossRef]
111. Singha, S.S.; Rudra, S.; Mondal, S.; Pradhan, M.; Nayak, A.K.; Satpati, B.; Pal, P.; Das, K.; Singha, A. Mn incorporated MoS_2 nanoflowers: A high performance electrode material for symmetric supercapacitor. *Electrochim. Acta* **2020**, *338*, 135815. [CrossRef]
112. Charapale, M.R.; Shembade, U.V.; Ahir, S.A.; Kothavale, V.P.; Jadhav, N.T.; Sankpal, V.G.; Waifalkar, P.P.; Moholkar, A.V.; Dongale, T.D.; Masti, S.A. Enhancing capacitive performance of MoS_2 through Fe doping: Synthesis, characterization, and electrochemical evaluation for supercapacitor applications. *Surf. Interfaces* **2024**, *52*, 104814. [CrossRef]
113. Khichi, P.; Siwach, P.; Gaba, L.; Kumar, V.; Kumar, J.; Ohlan, A.; Tripathi, R. Investigating and optimizing the variation of selenium infused MoS_2 as electrode material for supercapacitor applications. *FlatChem* **2024**, *46*, 100688. [CrossRef]
114. Zhang, H.; Wei, J.; Yan, Y.; Guo, Q.; Xie, L.; Yang, Z.; He, J.; Qi, W.; Cao, Z.; Zhao, X.; et al. Facile and scalable fabrication of MnO_2 nanocrystallines and enhanced electrochemical performance of MnO_2/MoS_2 inner heterojunction structure for supercapacitor application. *J. Power Sources* **2020**, *450*, 227616. [CrossRef]
115. Manuraj, M.; Chacko, J.; Unni, K.N.N.; Rakhi, R.B. Heterostructured MoS_2-RuO_2 nanocomposite: A promising electrode material for supercapacitors. *J. Alloys Compd.* **2020**, *836*, 155420. [CrossRef]
116. Saravanakumar, K.; Prasath, J.; Rajesh, R. Synthesis of SnO_2 and MoS_2 nano composites for supercapacitor applications. *Mater. Today Proc.* **2021**, *46*, 8189–8195. [CrossRef]
117. Rafique, K.; Hassan, N.; Shah, M.Z.U.; Al-Saeedi, S.I.; Shah, A.; Shah, M.S.U.; Aziz, U.; Sajjad, M.; Alanazi, A.A.; Hassan, H.M.A. Improved performance in asymmetric supercapacitors using SnO_2–MoS_2 composite microspheres. *Surf. Interfaces* **2024**, *44*, 103650. [CrossRef]
118. Salunkhe, T.T.; Bathula, B.; Kim, I.T.; Thirumal, V.; Yoo, K. Synergistic integration of MoS_2 nanopetals and SnO_2 quantum dots for enhanced supercapacitor performance. *J. Electroanal. Chem.* **2024**, *970*, 118562. [CrossRef]
119. Iqbal, M.; Saykar, N.G.; Arya, A.; Banerjee, I.; Alegaonkar, P.S.; Mahapatra, S.K. High-performance supercapacitor based on MoS_2@TiO_2 composite for wide range temperature application. *J. Alloys Compd.* **2021**, *883*, 160705. [CrossRef]
120. Ma, Y.; Jia, Y.; Lin, Y.; Shi, W. ZnS/MoS_2 film grown on Mo foil as binder free electrode for supercapacitor. *Chem. Phys.* **2021**, *542*, 111030. [CrossRef]
121. Liu, Y.; Sun, J.; Lin, S.; Xu, Z.; Li, L. In-situ growth of interconnected NiS_2/MoS_2 nanowires supported on Ni foam as binder-free electrode for hybrid supercapacitor. *J. Alloys Compd.* **2020**, *820*, 153113. [CrossRef]
122. Wang, Y.; Xie, Y. Electroactive FeS_2-modified MoS_2 nanosheet for high-performance supercapacitor. *J. Alloys Compd.* **2020**, *824*, 153936. [CrossRef]
123. Wan, L.; Liu, J.; Li, X.; Zhang, Y.; Chen, J.; Du, C.; Xie, M. Fabrication of core-shell $NiMoO_4$@MoS_2 nanorods for high-performance asymmetric hybrid supercapacitors. *Int. J. Hydrogen Energy* **2020**, *45*, 4521–4533. [CrossRef]
124. Wu, J.; Hu, G.; Zhao, J.; Zou, C.; Xing, H.; Shen, W.; Li, Z.; Liu, H. Hierarchical flower bud-like P, W co-doped $NiCo_2S_4$@MoS_2 composites as high-performance electrodes for asymmetric supercapacitor. *Appl. Surf. Sci.* **2024**, *663*, 160136. [CrossRef]
125. Fu, H.; Zhang, X.; Fu, J.; Shen, G.; Ding, Y.; Chen, Z.; Du, H. Single layers of MoS_2/Graphene nanosheets embedded in activated carbon nanofibers for high-performance supercapacitor. *J. Alloys Compd.* **2020**, *829*, 154557. [CrossRef]
126. Yang, W.; Hu, Z.; Zhang, C.; Guo, Y.; Zhao, J. Screen printing preparation of high-performance flexible planar micro-supercapacitors based on MoS_2 nanoparticles decorated electrochemically exfoliated graphene. *Electrochim. Acta* **2022**, *429*, 141041. [CrossRef]
127. Hota, P.; Miah, M.; Bose, S.; Dinda, D.; Ghorai, U.K.; Su, Y.-K.; Saha, S.K. Ultra-small amorphous MoS_2 decorated reduced graphene oxide for supercapacitor application. *J. Mater. Sci. Technol.* **2020**, *40*, 196–203. [CrossRef]
128. Sabeeh, H.; Zulfiqar, S.; Aadil, M.; Shahid, M.; Shakir, I.; Khan, M.A.; Warsi, M.F. Flake-like MoS_2 nano-architecture and its nanocomposite with reduced Graphene Oxide for hybrid supercapacitors applications. *Ceram. Int.* **2020**, *46*, 21064–21072. [CrossRef]
129. Bokhari, S.W.; Ellis, A.V.; Uceda, M.; Wei, S.; Pope, M.; Zhu, S.; Gao, W.; Sherrell, P.C. Nitrogen-doped reduced graphene oxide/MoS_2 'nanoflower' composites for high-performance supercapacitors. *J. Energy Storage* **2022**, *56*, 105935. [CrossRef]
130. Wang, H.; Tran, D.; Moussa, M.; Stanley, N.; Tung, T.T.; Yu, L.; Yap, P.L.; Ding, F.; Qian, J.; Losic, D. Improved preparation of MoS_2/graphene composites and their inks for supercapacitors applications. *Mater. Sci. Eng. B* **2020**, *262*, 114700. [CrossRef]

131. Pilathottathil, S.; Kavil, J.; Thayyil, M.S. MoS_2 incorporated carbon allotropes (activated carbon, graphene, MWCNT) as electrodes in symmetric supercapacitors. *J. Indian Chem. Soc.* **2021**, *98*, 100169. [CrossRef]
132. Kour, P.; Deeksha; Kour, S.; Sharma, A.L.; Yadav, K. Mixed-phase MoS_2 nanosheets anchored carbon nanofibers for high energy symmetric supercapacitors. *J. Energy Storage* **2023**, *63*, 107054. [CrossRef]
133. Tiwari, P.; Janas, D.; Chandra, R. Self-standing MoS_2/CNT and MnO_2/CNT one dimensional core shell heterostructures for asymmetric supercapacitor application. *Carbon* **2021**, *177*, 291–303. [CrossRef]
134. Chen, P.S.; Hu, Y.; Li, S.-Y.; Mazurkiewicz-Pawlicka, M. Artur Małolepszy, Preparation of a MoS_2/carbon nanotube nanocomposite by hydrothermal method for supercapacitor. *Int. J. Electrochem. Sci.* **2024**, *19*, 100523. [CrossRef]
135. Kumar, P.; Sharma, S.; Jabeen, S.; Samra, K.S. Hybrid microwave annealing assisted synthesis of MoS_2-RGO nanostructures: Optimization and characterization for application in supercapacitors. *Electrochim. Acta* **2022**, *426*, 140738. [CrossRef]
136. Farshadnia, M.; Ensafi, A.A.; Mousaabadi, K.Z.; Rezaei, B. Design and synthesis of three-dimensional $CoNi_2S_4$@MoS_2@rGO nanocomposites and its application in electrochemical supercapacitors. *J. Alloys Compd.* **2022**, *906*, 164278. [CrossRef]
137. Wei, W.; Liu, B.; Gan, Y.; Ma, H.; Chen, D.; Qi, J.; Li, S. One-step hydrothermal synthesis of Ni_3S_2/MoS_2 nanocomposites on rGO: Structural evolution and supercapacitor performance. *Surf. Coat. Technol.* **2020**, *403*, 126442. [CrossRef]
138. Serrapede, M.; Zaccagnini, P.; Rivolo, P.; Bianco, S.; Pirri, C.F.; Zampato, M.; Carminati, S.; Lamberti, A. The combination of MoS_2/reduced graphene oxide composite electrode and ionic liquid for high-temperature supercapacitor. *J. Energy Storage* **2023**, *73*, 109180. [CrossRef]
139. Yan, X.; Miao, J.; Wang, J.; Jiang, H.; You, M.; Zhu, Y.; Pan, J. High-performance polypyrrole coated MoS_2 nanosheets grown on carbon cloth as electrodes for flexible all-solid-state symmetric supercapacitor. *Mater. Sci. Eng. B* **2021**, *269*, 115166. [CrossRef]
140. Rajapriya, A.; Keerthana, S.; Viswanathan, C.; Ponpandian, N. Direct growth of MoS_2 hierarchical nanoflowers on electrospun carbon nanofibers as an electrode material for high-performance supercapacitors. *J. Alloys Compd.* **2021**, *859*, 157771. [CrossRef]
141. Arun, T.; Aravinth, K.; Bhargav, P.B.; Francis, M.K. Enhanced supercapacitor performance through surface modification: Binder-free electrode synthesis of Ni_3S_2/MoS_2/rGO on Ni-foam with superior cyclability. *J. Energy Storage* **2023**, *74*, 109333. [CrossRef]
142. Zhang, Y.; Feng, W.; Ma, M.; Zhang, N.; Ru, J.; Wang, X.; Zhang, Y.; Zhu, X. Heterostructure assembled by organic-molecule intercalated MoS_2 and reduced graphene oxide for enhanced interface energy and supercapacitor performance. *Surf. Interfaces* **2024**, *48*, 104373. [CrossRef]
143. Rani, S.; Bansal, L.; Bhatia, R.; Kumar, R.; Sameera, I. Engineered nano-architecture for enhanced energy storage capabilities of MoS_2/CNT-heterostructures: A potential supercapacitor electrode. *J. Energy Storage* **2024**, *84*, 110865. [CrossRef]
144. Liu, Z.; Xie, W.; Zhang, Z.; Mao, Y.; Zhan, T.; Zhang, D. 'MoS_2-coated nitrogen/oxygen co-doped carbon nanocages composite as active material for supercapacitor electrodes. *J. Solid State Chem.* **2024**, *331*, 124527. [CrossRef]
145. Aftab, J.; Ali, A.; Mehmood, S.; Aftab, A.; Ahmad, I.; Bhopal, M.F.; Hussain, M.; Shah, Z.U.; Shah, A.U.; Padhiar, M.A.; et al. Facile synthesis of synergetic MoO_2/MoS_2@GO nanohybrid as energy-efficient electrode material for high-performance asymmetric supercapacitor applications. *J. Energy Storage* **2023**, *74*, 109324. [CrossRef]
146. Khandare, L.N.; Mahabal, M.S.; Bhosale, S.R.; Late, D.J.; Kshirsagar, A.; Chaure, N.B. Facile synthesis and first principles calculations of Li-MoS_2/rGO nanocomposite for high-performance supercapacitor applications. *J. Energy Storage* **2024**, *102*, 114166. [CrossRef]
147. Li, L.; Wei, Z.; Liang, J.; Ma, J.; Huang, S. High-performance supercapacitor electrode materials of MoS_2/PPY nanocomposites prepared by in-situ oxidative polymerization method. *Results Chem.* **2021**, *3*, 100205. [CrossRef]
148. Wang, H. Silicon dioxide peristaltic supporting carbon and MoS_2 nanosheets co-anchored polyaniline for high-performance supercapacitors. *Synth. Met.* **2021**, *277*, 116772. [CrossRef]
149. Dai, J.; Luo, L.; Tang, Z.; Lv, Y.; Xie, H.; Zuo, H.; Yang, C.; Wang, X.; Fan, M.; Xu, Y.; et al. Strategy for constructing highly stable supercapacitors: Channeling of thin-layer polyaniline to enhance pseudo-capacitance of the CuS/polyaniline@MoS_2 composites. *Compos. Sci. Technol.* **2022**, *219*, 109240. [CrossRef]
150. Jasna, M.; Pillai, M.M.; Abhilash, A.; Midhun, P.S.; Jayalekshmi, S.; Jayaraj, M.K. Polyaniline wrapped carbon nanotube/exfoliated MoS_2 nanosheet composite as a promising electrode for high power supercapacitors. *Carbon Trends* **2022**, *7*, 100154. [CrossRef]
151. Suresh, S.; Sindhu, V. CeO_2/PANI/MoS_2 composite electrode for symmetric supercapacitor application. *J. Indian Chem. Soc.* **2022**, *99*, 100727. [CrossRef]
152. Jhanjhariya, N.; Lata, S. Potential window optimization to upgrade the performance of the designed triad MoS_2/MWCNT/PPy as an asymmetric supercapacitor device. *J. Energy Storage* **2024**, *82*, 110577. [CrossRef]
153. Pan, Z.; Li, X.; Yang, C.; Ji, X. One-step construction of $Ti_3C_2T_x$/MoS_2 hierarchical 3D porous heterostructure for ultrahigh-rate supercapacitor. *J. Colloid Interface Sci.* **2023**, *634*, 460–468. [CrossRef] [PubMed]
154. Qiao, Y.; Sun, W.; Yu, F.; Yu, J.; Yao, P.; Zhu, C.; Xu, J. Exploration of high performance and highly flexible supercapacitor configuration with MXene/1T-MoS_2 composite paper electrode. *Electrochim. Acta* **2023**, *464*, 142929. [CrossRef]
155. Li, H.; Lin, S.; Zhu, L.; Ru, J.; Ma, D.; Wang, X.; Li, B.; Zhang, Y.; Zhu, X. 3D heterostructure constructed by few-layer 1T MoS2 and MXene under high electrostatic fields for high-performance supercapacitors. *J. Power Sources* **2023**, *584*, 233627. [CrossRef]

156. Ali, S.; Javed, M.S.; Umer, K.; Wang, J.; Fu, Y.; Kong, S.; Khan, S.; Ahmad, A.; Parkash, A.; Albaqami, M.D.; et al. MoS_2@$Ti_3C_2T_x$ Heterostructure: A new negative electrode material for Li-Ion hybrid supercapacitors. *Chem. Eng. J.* **2024**, *498*, 155330. [CrossRef]
157. Bera, S.; Mondal, T.K.; Su, Y.-K.; Saha, S.K. Sulfur-tuned MoS_2 quantum dot decorated $Ti_3C_2T_x$ (MXene) electrode materials for high performance supercapacitor applications. *J. Alloys Compd.* **2024**, *985*, 174010. [CrossRef]
158. Hayat, H.P.; Dokan, F.K.; Onses, M.S.; Yılmaz, E.; Duran, A.; Sahmetlioglu, E. Flexible electrodes composed of flower-like MoS_2 and MXene for supercapacitor applications. *Mater. Res. Bull.* **2024**, *175*, 112747. [CrossRef]
159. Hou, W.; Sun, Y.; Zhang, Y.; Wang, T.; Wu, L.; Du, Y.; Zhong, W. Mixed-dimensional heterostructure of few-layer MXene based vertical aligned MoS_2 nanosheets for enhanced supercapacitor performance. *J. Alloys Compd.* **2021**, *859*, 157797. [CrossRef]
160. Radhakrishnan, S.; Lakshmy, S.; Raj, K.A.S.; Chakraborty, B.; Cho, J.S.; Jeong, S.M.; Rout, C.S. Facile and scalable fabrication of flexible microsupercapacitor based on boron modified 2D/2D 1 T MoS_2/MXene hybrids. *J. Energy Storage* **2024**, *99*, 113478. [CrossRef]

Disclaimer/Publisher's Note: The statements, opinions and data contained in all publications are solely those of the individual author(s) and contributor(s) and not of MDPI and/or the editor(s). MDPI and/or the editor(s) disclaim responsibility for any injury to people or property resulting from any ideas, methods, instructions or products referred to in the content.